Evolution of hydration in cement blends with incorporation of activated low-kaolinite clays: Insights into the preferred aluminum uptake by

Cement and Concrete Research 201 (2026) 108086

Contents lists available at ScienceDirect

Cement and Concrete Research

journal homepage: www.elsevier.com/locate/cemconres

Evolution of hydration in cement blends with incorporation of activated low-kaolinite clays: Insights into the preferred aluminum uptake by C-(A)-S-H

Amrita Hazarika [a,*], Liming Huang [a], Joao Figueira [b], Arezou Babaahmadi [a]

[a] Department of Architecture and Civil Engineering, Chalmers University of Technology, Gothenburg, 41279, Sweden
[b] Department of Chemistry, Scilife Lab, Umeå University, Umeå, 90187, Sweden

ARTICLE INFO

Keywords:
Low-kaolinite
Thermo-mechanical activation
NMR
Hydration
C-(A)-S-H

ABSTRACT

Despite their global abundance, heterogenous clays are often excluded from SCM applications, due to their limited pozzolanicity. This study investigates hydration evolution, particularly aluminum uptake pathways, in statistically designed cement blends incorporating thermo-mechanochemically activated low-kaolinite clays.

Despite kaolinite contents below 40%, a 30% binary blend achieved 110% and 125% of OPC strength at 7 and 56 days, respectively, while reducing total porosity by 42% at 56 days. ^{29}Si NMR indicated an increase in silicate chain length in C-(A)-S-H, correlating with pore structure refinement and strength gain in 56 days of hydration. ^{27}Al NMR revealed a preferential incorporation of aluminum into C-(A)-S-H rather than AFm phases. This behavior is attributed to the lower alumina availability in the system compared to LC3 blends, suggesting that in such environments, C-(A)-S-H becomes the dominant host phase for aluminum. This incorporation pathway reduces the Al availability for carbonate-AFm formation, limiting the synergy typically observed in LC3 systems with added limestone.

1. Introduction

Cement is the most widely manufactured material on Earth by mass, while also being one of the largest contributors to global carbon emissions [1]. Yet, as equitable global development demands the expansion of infrastructure, cement remains indispensable due to its affordability and energy efficiency. In 2022, the Global Cement and Concrete Association (GCCA) outlined seven pathways to achieve net-zero emissions in cement production and use [2]. Among them, the use of supplementary cementitious materials (SCMs) as partial clinker substitutes offers the most cost-effective and performance-compatible solution [1]. However, traditional and standardized SCMs like fly ash and blast furnace slag are becoming increasingly scarce to reduce future dependance on clinker. As a result, the focus has shifted to naturally available alternatives such as clays and limestone that have the potential to be applied globally [3].

An extensive body of research demonstrate the potentials of limestone calcined clay cement (LC3) systems, incorporating calcined clays together with limestone, to replace up to 50% of clinker while maintaining performance on hydration, mechanical properties, and durability [1,4–15]. These studies have explored clay treatment and activation, mineral characterization, pozzolanic reactivity, blend optimization, hydrate phase analysis, pore structure, ionic transport, and performance under various exposure conditions. While high grade metakaolin is expensive to produce, a consistent finding across this body of work is that a kaolinite content of at least 40% is essential for the effective use of calcined clay as an SCM. This is driven by kaolinite's higher aluminosilicate content and hydroxyl structure that facilitates high reactivity upon calcination and promotes the formation of carboaluminates with carbonates from limestone that improve strength as well as durability [10,16].

However, most global clay resources contain less than 40% kaolinite and are instead dominated by a mix of less reactive 2:1 clay minerals and other non-clay minerals often considered impurities [17]. For example, most clay resources in the Nordic [18–21], parts in UK [22], South-East European regions [23], central Italy [24], as well as southern African regions such as Angola and Zambia [25], have no more than 25% kaolinite. These clays are often multi-phase or heterogenous, instead of pure phase clays studied earlier. Therefore, while clay is abundant globally, the predominantly suggested clays with at least 40% kaolinite content, are not universally representative. Therefore, findings based on kaolinite-rich clays cannot be broadly applied to all clay types in current or future standards, especially in above-mentioned regions. Further and continued research on low-kaolinite, less reactive clays is vital to fully realize the potential of clays as SCMs.

* Correspondence to: Department of Architecture and Civil Engineering, Chalmers University of Technology, SE-412 96 Gothenburg, Sweden.
E-mail address: amrita.hazarika@chalmers.se (A. Hazarika).

https://doi.org/10.1016/j.cemconres.2025.108086
Received 7 August 2025; Received in revised form 31 October 2025; Accepted 8 November 2025
Available online 12 December 2025

Table 1
Chemical composition (by weight percentage) of binders.

Binder	SiO_2	Al_2O_3	Fe_2O_3	CaO	MgO	Na_2O	$CaCO_3$	LOI	Total (%)	d50 (μm)
Natural Clay (CC)	51.80	18.35	9.55	1.32	3.34	1.70	–	8.15	99.86	16.00
CEM I (OPC)	19.60	4.50	3.00	63.50	3.50	0.27	–	2.50	99.53	–
Limus 15 (LS-L)	7.00	0.70	0.30	50.50	0.50	0.10	90.00	–	100.00	41.70
KÖ100 (LS-M)	5.50	1.40	1.50	48.50	2.50	0.10	87.50	–	100.00	15.10
Enrich C (LS-F)	< 0.01	<0.01	< 0.01	< 0.01	<0.01	< 0.01	> 99.00	–	>99.00	0.10

Several studies have explored low-reactive clays, proposing activation strategies to enhance their pozzolanic and blended reactivity [21,26–32]. Other works have examined the influence of activated 2:1 clays or low-grade kaolinites on OPC hydration [26] and durability [22,33]. These studies generally show that while mechanical performance can improve with activation, blends using low-reactive clays rarely match OPC strength, or do so only at later ages. This is often attributed to the low aluminosilicate content and the difficulty in fully dehydroxylating clay minerals during calcination. It is also due to the low aluminate levels in such clays that synergy with carbonates from limestone is reported to be limited compared to clays with high kaolinite contents [22,34]. This is due to the slower aluminate release from 2:1 clay minerals compared to kaolinite [35].

To address these limitations, mechanochemical activation (MCA) has emerged as a promising alternative to calcination. MCA can induce greater structural disorder and enhance reactivity, especially in mineralogies where thermal activation alone is insufficient [27]. However, its effectiveness varies depending on the specific clay composition. Our previous research demonstrated that MCA alone may not be universally effective across all low-reactive clays. Instead, our previous work showed that combining calcination at 800 °C with 20 min of MCA at 500 rpm significantly improves the physico-chemical properties of heterogeneous clays, including those containing low-grade kaolinite, smectites, illites, and non-clay minerals [36]. This combined activation approach resulted in up to 127% increase in reactivity, effectively addressing the activation challenge for such clays. With activation optimized, the next critical step is to evaluate whether these improvements translate into viable binder performance. Specifically, it is essential to determine how much cement can be replaced by the activated clay and whether limestone can serve as a suitable third component in ternary blends. Given the lower aluminum content in these clays, it remains unclear whether sufficient carboaluminate formation can occur, or if aluminum preferentially enters other hydrate phases such as C-(A)-S-H. Existing LC3 mix designs, developed for high-kaolinite clays, cannot be directly applied to these systems.

Building directly on our previous work [36], where the combined activation strategy enhanced key properties such as particle fineness, amorphization, and pozzolanic reactivity, the current investigation shifts focus from activation to binder design. A statistically defined binder design was developed to generate a representative range of binary and ternary blends across specific levels of CEM I substitution with a thermo-mechanochemically activated heterogeneous natural clay. This framework enables systematic evaluation of limestone synergy and aluminum incorporation mechanisms in low-kaolinite systems. Compressive strength, pore structure development, and hydrate assemblage are assessed to determine how these blends perform relative to conventional LC3 systems. While durability testing is beyond the scope of this work, the selected parameters serve as critical indicators of binder quality and long-term potential. Ultimately, the aim is to establish a robust binder design strategy tailored to the unique characteristics of underutilized clay resources, contributing to performance optimization and a deeper understanding of hydration mechanisms in low-aluminate SCM systems.

To investigate the hydration behavior and performance of the designed blends compressive strength tests were conducted on mortar blends at 3, 7, 28, and 56 days. Mercury intrusion porosimetry (MIP) was employed to analyze the evolution of pore structure in hardened mortars. Hydrate phase assemblages were characterized using X-ray diffraction (XRD), thermogravimetric analysis (TGA), while ^{29}Si and ^{27}Al solid-state nuclear magnetic resonance (NMR) spectroscopy was employed to investigate the structural environments of silicon and aluminum species. Finally, isothermal calorimetry was employed to specifically assess the role of limestone particle size on reaction kinetics, as well as to evaluate the kinetics of sulfate depletion.

2. Materials and methods

2.1. Materials

The clay used for this study is a glacial type and was sourced from eastern marine region of Norrköping in Östergötland, in Sweden. Through previous research [36] the clay was found to contain 21 ± 2% kaolinite, 28 ± 2% smectite and 33 ± 2% illite with a total clay content of 82 ± 2%. The remaining fractions of the glacial marine deposited clay in this region is known to be mainly silt with small amounts of fine sand [20]. Portland cement CEM I 52.5 R was obtained from Skövde, Heidelberg Materials, Sweden. Limestone used for casting mixes was Limus 15, obtained from Nordkalk AB, Ignaberga, Sweden. Additionally, two more limestone types from Nordkalk (KÖ100, and Enrich C powder) with varying particle size distributions were also used for assessing the effect of limestone particle size on reaction kinetics. The chemical composition of the binders used, obtained from Inductively coupled plasma atomic emission spectroscopy (ICP-AES) are provided in Table 1. For mortars, the aggregate used was CEN-NORMSAND which is packeted with grain size distributions conforming to EN196-1. A Polycarboxylate ether (PCE) based superplasticizer was used for the clay mixes, which was designed and provided by Sika, Switzerland. It contained a patented clay blocker molecule, that blocks PCE adsorption on clay surfaces, allowing effective clay particle dispersion and improved workability compared to conventional PCEs designed only for cement. Isopropanol (2-propanol, ACS reagent > 99.5% purity, Sigma Aldrich) was used for hydration stoppage.

2.2. Binder mix designing

Binder mixes were composed of OPC, activated clay, and limestone. A statistical mixture design approach was used to explore possible binder combinations efficiently. The mix proportions were generated using the Scheffe quartic model in the Optimal (Custom) Design mode of the Design-Expert v22.0 (Stat-Ease 360) software. A Scheffe quartic model can handle complex, nonlinear interactions between components [37]. It includes not only single and pairwise effects but also higher-order interactions, such as in ternary mixes where all three materials may influence performance together or synergistically [38,39].

The following constraints were applied for the binders: OPC (50%–100%), clay (0%–50%), and limestone (0%–50%), where the total always summed to 100%. OPC replacement above 50% was avoided to maintain enough calcium hydroxide (CH) for pozzolanic reaction with clay [40]. Substitution below 20% was also excluded, as it would have little environmental benefit.

From the suggested mixes from the software we excluded the repetitive or unrealistic combinations in which the portion of limestone was higher than clay. It is reported that the presence of additional limestone would likely behave as unreacted fillers after available alumina is used

Table 2
Mixes used in the study and their corresponding proportions.

No.	Mix name	CEM I (OPC) wt %	Activated clay (CC) wt %	Limestone (LS) wt %
1	OPC	100	0	0
2	CC20	80	20	0
3	CC30	70	30	0
4	CC40	60	40	0
5	CC50	50	50	0
6	CC20LS10	70	20	10
7	CC30LS10	60	30	10
8	CC40LS10	50	40	10
9	CC20LS20	60	20	20
10	CC30LS20	50	30	20
11	CC20LS30	50	20	30
12	LS20	80	0	20
13	LS30	70	0	30
14	LS40	60	0	40
15	LS50	50	0	50

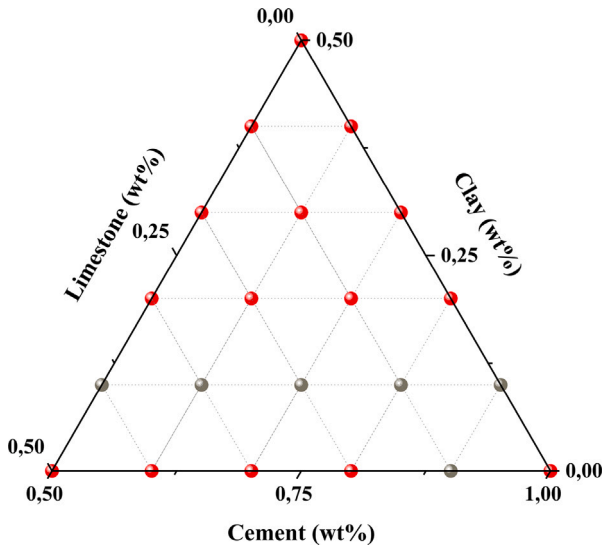

Fig. 1. Ternary plot representing the design space for the mix proportions according to Scheffe quartic model. Of the 32 mixes generated by the model, 11 were repetitive. As such the plot shows 21 unique points, of which 15 were selected for the current study, represented by the red dots. (For interpretation of the references to color in this figure legend, the reader is referred to the web version of this article.)

up, leading to dilution and loss of strength [6,41,42]. However, a few such combinations were retained for statistical balance.

Fig. 1 shows the ternary plot of all modeled mixes, with red dots indicating those selected for testing and gray dots representing excluded ones. Table 2 presents the mix proportions corresponding to the red dots in Fig. 1. This approach enabled a targeted and statistically balanced mix selection, ensuring that the experimental program investigates a broad but practical range of binder proportions. The robustness and interpolation capacity of the model were assessed with ANOVA with the responses obtained from strength and pore structure measurements.

2.3. Sample preparation

The raw clay was treated and activated in the combined thermal and mechanochemical (TA-MCA20) method established in [36]. After combined TA-MCA20, which included thermally activating the clay at 800 °C followed by mechano-chemical activation for 20 min at a speed of 500 rpm and ball to powder ratio of 25, the d50 of the clay was 16 ± 1 μm, SSA was 18.5 ± 2 m2/g, and Degree of Amorphization (DOA) was 83 ± 3%. The mineralogy of the raw clay and the effect of activations on the clay particle parameters are provided in supplementary material (sections 1 and 2).

For assessing compressive strength developments, mortars were prepared for four ages (3, 7, 28 and 56 days). The mortars were mixed in an automatic mortar mixer (Auto-Mortar Mixer), programmed according to mortar mixing steps outlined in Standard EN 196 [43]. Thereafter, they were cast in 40 × 40 × 40 mm molds as against prism molds suggested in EN 196, for ensuring judicious use of the binder material. For mixing, a constant water to binder ratio of 0,5 was used for all mixes. Additionally, a PCE based superplasticizer with 2% by weight of clay was used for mixes containing clay. The cubes were cured under 100% relative humidity at 20 ± 1 °C, until the age for strength testing. Three samples of every proportion were cast for representativeness. After strength tests, pieces of mortar, of size around 5 cm were collected from each sample to stop hydration by immediately immersing in isopropanol. After hydration stoppage, these samples were further clipped to 3 mm to conduct MIP tests.

The hydrate phase characterization was conducted on hardened pastes which were prepared by mixing 120 g of binder, 60 g of water and proportionately the PCE superplasticizer for clay-based binders. Mixing was done with a handheld blender (Bosch ErgoMix 800 W) for 2 min, after which the mix was poured in four 15 ml centrifuge tubes. The tubes were vibrated for 5 s and sealed tightly. Thereafter, they were mounted on bench top mini rotators (Fischer Scientific) at 35 rpm and left overnight to mix. After 24 h, the seals were taken out and the tubes were left to cure in 100% relative humidity till the relevant age of 3, 7, 28 or 56 days. At the relevant age, the paste was demolded from the plastic tube and crushed to smaller pieces of around 5 mm.

For hydration stoppage, samples of both mortar and pastes were immersed in isopropanol inside 50 ml centrifuge tubes and stored for 7 days. The isopropanol was replaced daily to ensure effective stoppage. After 7 days, the samples were removed from the isopropanol and dried in a vacuum oven at 30 °C until completely dry. For MIP tests, the dried mortar pieces were clipped with a metal shearing scissor to smaller pieces of approximately 3 mm. Up to 12 pieces were collected from every mix for MIP testing.

2.4. Characterization methods

Strength test was conducted on compression testing machine (Matest 300 kN). MIP was conducted on a MicroActive Autopore V 9620 instrument. A mercury intrusion pressure of 60000 psi (413.68 MPa) and a contact angle of 130° was used for the measurements.

For hydration characterization, the dried paste samples were then ground using a mortar and pestle until the powder could pass through a 75 μm sieve. The resulting powder was either used immediately for measurements or stored in a desiccator with silica gel, for later use.

XRD was conducted on BrukerD8 Discover in the 2 theta range 5–60 °θ with a step size: 0.02 °θ, and time per step of 0.8 s TGA was conducted on TGA/DSC 3+ Mettler Toledo, in a Nitrogen flow of 50 mL/min, heating from 20 to 1000 °C with a rate of 10 °K/min.

The silicon and aluminum state in selected hydrated pastes were measured by ^{29}Si and ^{27}Al solid-state nuclear magnetic resonance spectroscopy (NMR), to investigate the distribution and incorporation of Al in C-(A)-S-H and AFms. Both the ^{29}Si and ^{27}Al MAS NMR spectra were obtained using a Bruker 4 mm MAS BB/1H probe at 298 K. Samples of 0.09 g were packed in 4 mm zirconia rotors. The ^{29}Si high-powered decoupled (HPDEC) MAS NMR spectra were acquired at 2500 scans at a spin rate of 7.5 kHz. This used a 3 μs pulse, corresponding to an excitation angle of about 450 and a relaxation delay of 30 s. The ^{27}Al (HPDEC) MAS NMR used a total of 2048 scans at a spin rate of 11 kHz, using a 4 μs pulse corresponding to an excitation angle of about 650 and a relaxation delay of 0.8 s. Both experiments used SPINAL64 proton decoupling with a 1H-field strength of 50 kHz [44]. The deconvolutions were conducted on the Interactive Peak Fitting (IPF, Version 13.2.0.0) software that were run on Matlab 2024b [45]. The Al/Si ratios and mean chain lengths (MCL) of aluminosilicate tetrahedra were calculated using the following Eqs. (1) and (2), as reported previously in [46,47]:

$$\mathrm{Al/Si} = \frac{Q_p^2(1\mathrm{Al}^{\mathrm{IV}})}{2[Q^1 + Q_p^2(1\mathrm{Al}^{\mathrm{IV}}) + Q^2]} \quad (1)$$

$$\mathrm{MCL} = \frac{2\left(Q^1 + \frac{3}{2}Q_p^2(1\mathrm{Al}^{\mathrm{IV}}) + Q^2\right)}{Q^1} \quad (2)$$

Mixes for calorimetry were prepared with 5 g of binder and 2.5 g of deionized water, according to the proportions for each mix. Two sets of each mix underwent 60 s of stirring for thorough mixing in a vortex mixer and were then placed in an isothermal calorimeter (Calmetrix) at 20 °C for up to 7 days. An average of the two sets of results for every mix was plotted for results. The standard deviation was < 5% that ensured good repeatability. To assess strength and pore structure, all mixes listed in Table 2 were tested. For XRD and TGA analyses, a subset of mixes (OPC, CC30, CC40, CC50, CC20LS10, CC30LS10, and CC40LS10) was selected to represent binary and ternary systems across increasing replacement levels. For ^{29}Si and ^{27}Al NMR characterization, matured ages of one binary blend, CC30, and one ternary blend CC20LS10 were considered. They were chosen as they showed the highest strength and lowest porosity in their respective binder groups, along with measurable CH and AFm (Hc and Mc) phases. Of the two, only CC30 was used for deconvolution and calculation of C-(A)-S-H chain lengths, as it showed a clear enhancement in aluminum incorporation. This blend was therefore considered most representative for qualitatively examining Al incorporation pathways and as a potential candidate for future durability assessments.

3. Results

This section presents the independent experimental results on strength development, reaction kinetics, hydrate phase assemblage, pore structure, and the structural environments of silicon and aluminum. The relationships and implications of these results are then discussed in the subsequent section.

3.1. Compressive strength

The compressive strength evolution for all mixes at four curing ages are presented in Fig. 2. Corresponding bar charts for each age are provided in Fig. A.13 of Appendix A. In Fig. 2 warmer color shades (orange to red) represent higher strength in contrast to the cooler shades (green to blue) primarily observed in the 3- and 7-day strengths. The ternary plots suggest that the blends react differently in relation to the proportions of clay and limestone present. Most notably, the binary clay binders show faster strength development over the four ages, even at high replacement ratios. In contrast, the presence of limestone in clay blends, is not observed to result in any enhancement of strength development, as traditionally observed in the case of LC3 systems [6,48]. Limestone–cement binders show lower strength at all ages than clay-cement blends, highlighting the pozzolanic effect of the activated clays.

In particular, it is observed that already from 7 days, CC20 and CC30 exhibit higher strength compared to 100% OPC. By 56 days, these two mixes achieved 69 ± 1.0 MPa and 76 ± 1.0 MPa, representing 113% and 125% of OPC strength respectively. From 28 days, CC40 also achieves strength levels equal to OPC. At the same time CC50 attains a compressive strength up to 87% of OPC. By 56 days, CC40 attains 102% and CC50 achieves 85% of OPC strength.

Among the ternary blends evaluated, only CC20LS10 and CC30LS10 achieved compressive strengths comparable to OPC from 28 days onward, with CC40LS10 attaining 81% strength of OPC at 56 days. The presence of lower aluminate levels in the clay compared to those used for LC3 binders with higher kaolinite contents [6,42], possibly hinders the synergistic interactions with the carbonates from added limestone.

The strength evolution was analyzed with Analysis of Variance (ANOVA) to evaluate statistical significance of the mixes and interactions in predicting the strength response for the studied blends. The ANOVA results confirmed that the model was highly significant, with a model R^2 of 0.956, F-value of 70.07 indicating there is less than a 0.01% chance that the model fit could occur due to random variation. Furthermore, a Predicted R^2 value of 0.91 and a Predicted Residual Sum of Squares (PRESS) value of 308.68 indicates that the model has good interpolative capacity, suggesting that it can reliably estimate responses at untested points within the experimental design space [49]. The results of the analysis are provided in supplementary materials.

3.2. Pore structure

Fig. 3 presents the evolution of total intruded porosity across hardened paste matrix. The densification over curing age can be clearly observed for all mixes, particularly in the clay mixes, among which, the evolution for binary mixes is most significant. CC30 has the highest reduction of total porosity from 3 to 56 days among all mixes, with a decrease of 42% (from 18.5% at 3 days to 10.7% at 56 days). Compared to strength evolution of the matrix presented in Fig. 2, the mixes with the higher strength roughly correspond to that with the lower porosity presented in Fig. 3. A bar chart of total porosity and total pore volumes in each age for the mixes are presented in Fig. B.16 (a,b) of Appendix B.

However, a good correlation between compressive strength and total porosity or total pore volumes, was not observed statistically (Fig. B.17 in Appendix B). In this context, previous studies [50,51] have highlighted the need to differentiate the pore size ranges to separate the effect of different pore sizes on the compressive strength. Fig. 4 (a–c) shows the evolution of pore size distribution for OPC, two binary blends, two ternary blends and two filler blends. The remaining mixes are presented in Fig. B.15 in Appendix B. The pore sizes are categorized into 5 ranges from below 0.01 μm to 100 μm. Three broad size distribution categories are considered from the studies of [52,53]: (1) gel pores or micro pores (< 0.01 μm), (2) capillary or meso pores (0.01–10 μm) which is further subdivided into small capillary pores (0.01–0.1 μm), medium capillary pores (0.1–1 μm) and large capillary pores (1–10 μm), (3) macro pores (10–100 μm) that are typically developed due to inadequate compaction or entrained air. Out of these, a higher percentage of capillary and macro pores are reported to be detrimental for strength and elasticity [52].

From Fig. 4, after 3 days of curing, all blended mixes are observed to have higher total pore volumes compared to references (OPC). Comparatively, filler mixes LS20 and LS30 are observed to have lower pore volumes than OPC. However, compressive strengths of mix only with

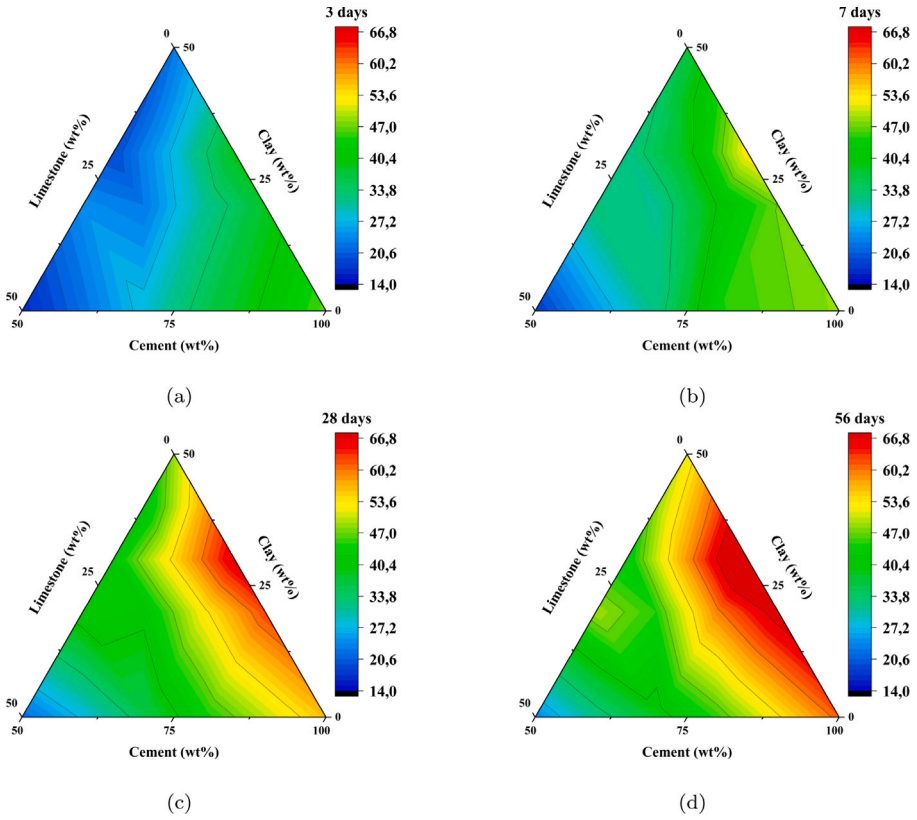

Fig. 2. (a–d): Compressive strength evolution of the matrix over time at 3, 7, 28 and 56 days.

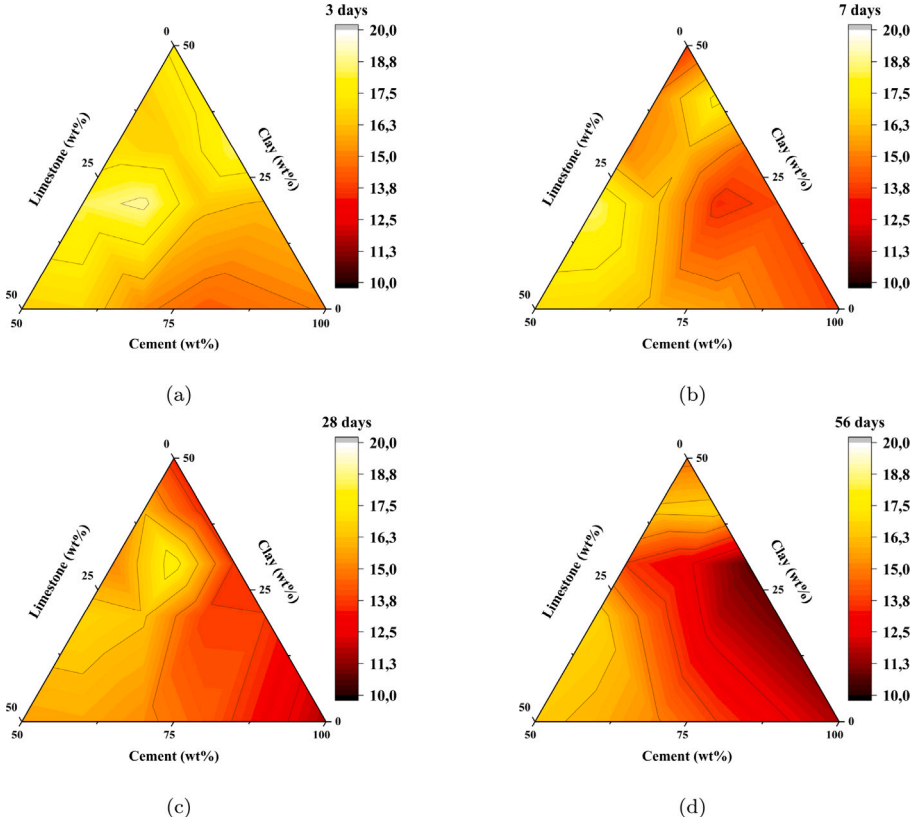

Fig. 3. (a–d): Evolution of porosity of hardened matrix at 3, 7, 28 and 56 days.

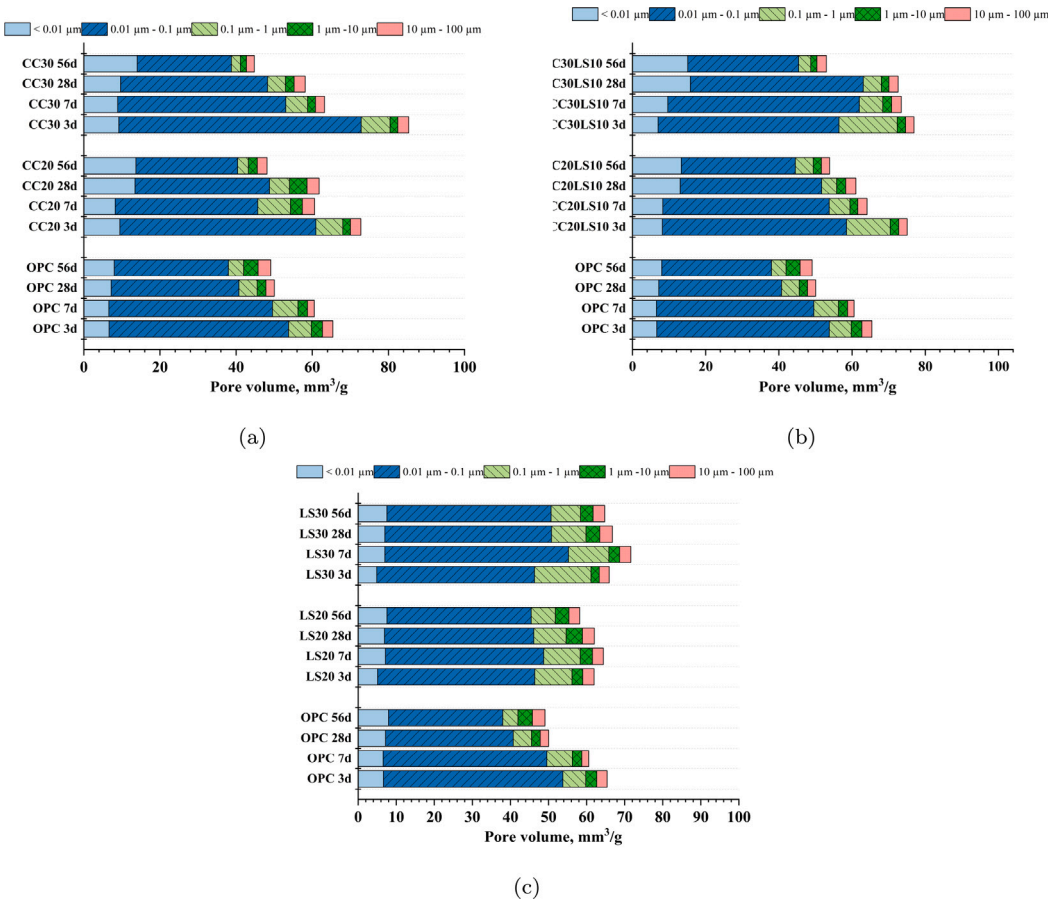

Fig. 4. Distribution of pore volumes of reference (OPC), binary mixes with activated clay (a), ternary mixes (b), and limestone fillers (c).

fillers are much lower than both the OPC and clay mixes, especially the binary mixes of CC20, CC30. It is noteworthy that mixes CC20, CC30, CC20LS10 and CC30LS10 have a higher volume of small pore sizes, especially in gel or micro pore range, compared to OPC. Fig. 5 shows the statistical correlation between strengths and the pore volumes of the mixes across all curing ages. It is seen that the gel porosity alone did not correlate well with strength development. It should also be noted that mercury intrusion porosimetry captures only pore-entry diameters rather than the full connectivity of the pore network [54]; therefore, apparent micro-pore increases may not always reflect reduced permeability. R^2 for the correlation between strength and gel pore volumes is only 0.40, while the best correlation was observed for medium capillary pores with the size range 0.1–1 μm (100–1000 nm), with a R^2 value of 0.99. This indicates a higher potential of this size range to control strength in the studied mixes.

ANOVA was conducted on the 56 days pore structure results (details are provided in Supplementary Material, Section 4). The total porosity showed undefined predictability. The gel pore volume had R^2 0.97 and adjusted R^2 of 0.91. The total capillary pore volume had R^2 of 0.99 and adjusted R^2 of 0.99. The medium (0.1–1 μm) capillary pore volume had predicted R^2 of 0.89 and adequate precision = 22.7 [49]. For gel pore volumes, the cement–clay interaction had F = 29.81 and the cement–limestone interaction F = 10.48. For total capillary pore volume, the cement–limestone interaction had F = 635.44. For medium capillary pore volume, the clay–limestone combination had F = 36.86 ($p = 1.62 \times 10^{-5}$), the cement–clay interaction F = 8.02 (p = 0.012), and the cement–limestone interaction p = 0.0586.

3.3. Reaction kinetics

Fig. 6 shows the hydration heat flow (a) and cumulative heat release up to one week (b) for OPC, binary (CC20, CC30, CC40), and ternary (CC20LS10, CC30LS10, CC40LS10) blends. The results are normalized to per gram of OPC. Compared to the reference, a higher silicate reaction peak is observed for all blended binders, primarily because of filler effect and faster precipitation of C-(A)-S-H due to the increased shear rate between particles as proposed earlier by [55,56] and the additional nucleation surfaces provided by the SCMs [54,57]. The onset and intensity of the aluminate peak appears to be varied across the blends.

All blends exhibit the characteristic silicate hydration peaks, with the main peak intensity decreasing and shifting to later times as the cement replacement increases. Among the clay blends, CC30 shows the highest main peak and cumulative heat. Ternary blends release slightly more total heat than their corresponding binaries at equivalent replacement levels. Overall, all substituted systems display continued heat evolution beyond the main hydration peak, indicating sustained reaction activity at later ages.

Additionally, Fig. 7 shows the reaction kinetics of two ternary blends, CC20LS10 and CC30LS10, prepared with limestones of different particle-size distributions. The d50 of the limestones used are: LS-L = 40 μm, LS-M = 15 μm, LS-F = 0.1 μm. The finer limestone (LS-F) produces a higher and earlier main hydration peak, indicating accelerated early C_3S reaction. The cumulative heat release follows the order of fineness, with coarser limestone showing lower and delayed heat evolution.

3.4. Hydrate phase assemblage

Fig. 8 illustrates the XRD patterns of the cement pastes cured for 3, 7, 28, and 56 days. This analysis focuses on binary and ternary blends with 30%, 40%, and 50% cement replacement levels, in comparison to the 100% OPC reference. Across the blends of all curing durations,

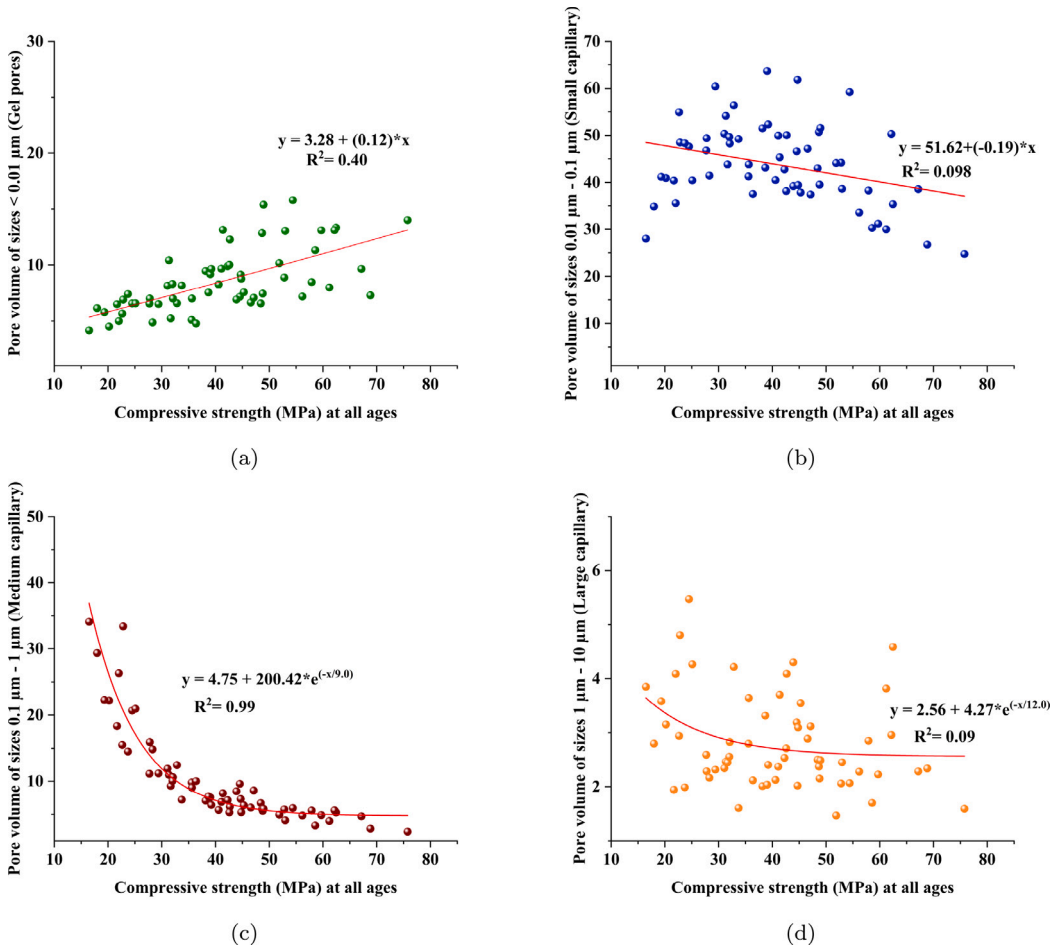

Fig. 5. Correlation between strength and gel pore volumes (a), small capillary volumes (b), medium capillary pore volumes (c) and large capillary pore volumes (d). The R2 of all the correlations are presented.

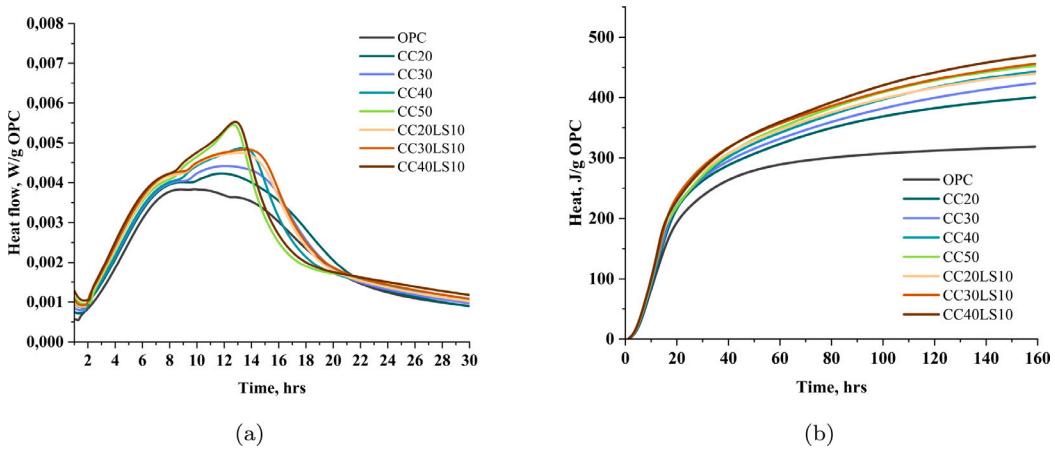

Fig. 6. Hydration heat flow of blends (a), and cumulative heat till 1 week of measurement (b).

phases such as ettringite, portlandite (CH), and CO_3-AFms (both hemicarboaluminate (Hc) and mono-carboaluminate (Mc)) are consistently observed, albeit with varying peak intensities.

Fig. 9 presents the CH peak intensities for 30, 40, and 50% replacement levels at 3 and 56 days. CH intensity decreases with increasing replacement and curing age due to progressive consumption by pozzolanic reactions. At 3 days, LS30 shows higher CH intensity than OPC, attributed to the calcite-induced acceleration of C_3S hydration [56, 58,59]. The binary clay blends (CC30 and CC40) show lower CH intensities, while ternary blends such as CC20LS10 and CC30LS10 exhibit slightly higher values because of the additional limestone surface available for C_3S hydration.

Moreover, CH is also consumed during the formation of hemicarboaluminates [60]. Fig. C.18 in Appendix C shows the intensities of the CO_3-AFm phases. It is observed that the binary clay binders have a higher intensity of Hc at 3 days compared to both ternary, as well as LS binary blends. Correspondingly, the CH intensities of CC30 and CC40 are lower than LS30 or LS40 at 3 days, as well as CC20LS10

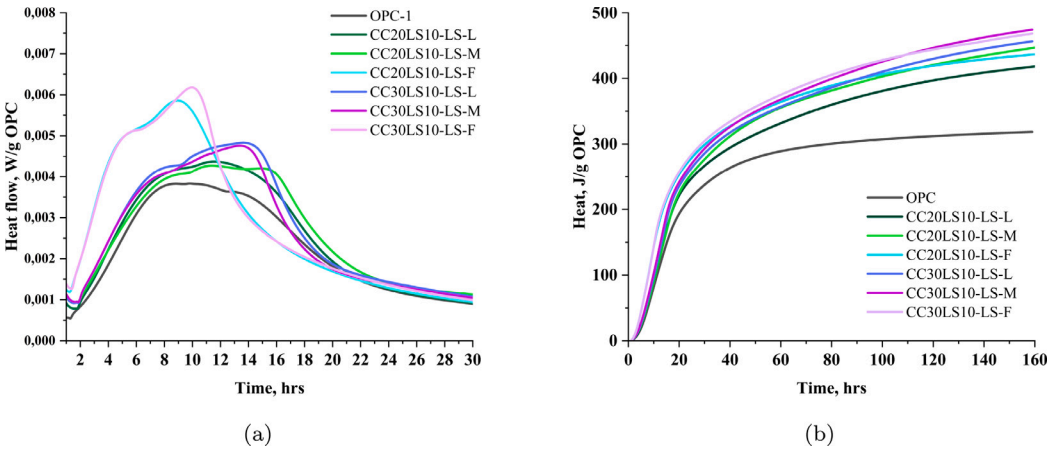

Fig. 7. Study of reaction kinetics with heat flow (a) and cumulative heat evolution (b) for CC20LS10 and CC30LS10 containing limestones of different PSD, specifically, LS-L, LS-M and LS-F.

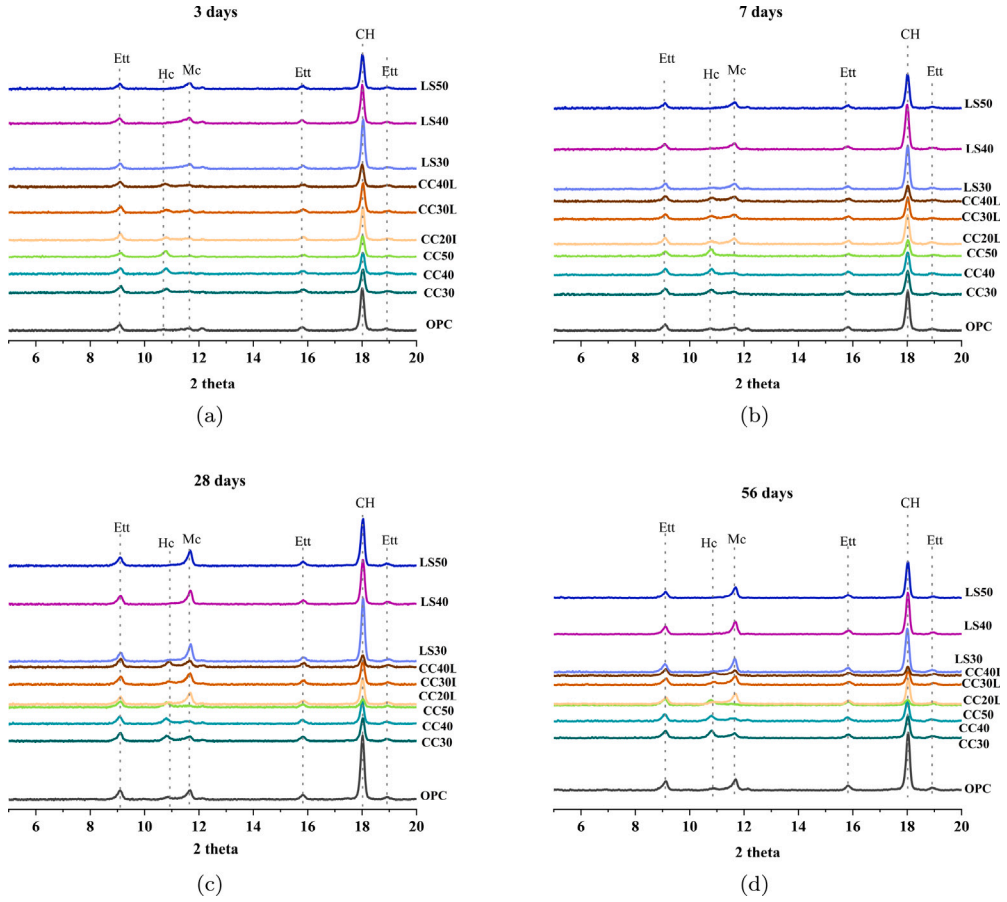

Fig. 8. XRD of selected blends and the corresponding limestone replacements, at four curing ages. The notations are as follows: Ett = Ettringite, Hc = Hemicarbonates, Mc = Monocarbonates, CH = portlandite.

and CC30LS10. With curing, Hc intensity decreases and Mc intensity increases, indicating transformation to the thermodynamically stable carbonate-AFm phase [61,62]. Ternary mixes display more pronounced Mc reflections at later ages due to greater calcite availability.

Both binary and ternary CC blends, despite their lower kaolinite content, show formation of Hc and Mc. The overall quantity of CO_3-AFms is lower than would be expected in kaolinite-rich systems, which is consistent with earlier observations on mixed-layer natural clays reported by Beuntner [34]. This behavior reflects the slower aluminate release from 2:1-type clays compared with kaolinite [35].

Fig. 10(a) presents the proportion of CH (corresponding to mass loss in the range 400–500 °C), and Fig. 10(b) shows the hydrate water proportions (corresponding to mass loss in the range 40–520 °C), for mixes corresponding to 30% substitution, as computed from the TGA. The remaining substitutions are presented in Fig. C.19 in Appendix C. The DTG curves for the blends are presented in Fig. C.20 (a–d) of Appendix C. Some carbonates (in the range of 520–820 °C) are observed even in blends without added limestone, which could be a result of approximately 5% limestone present in the cement, along with possible carbonation during preparation and curing.

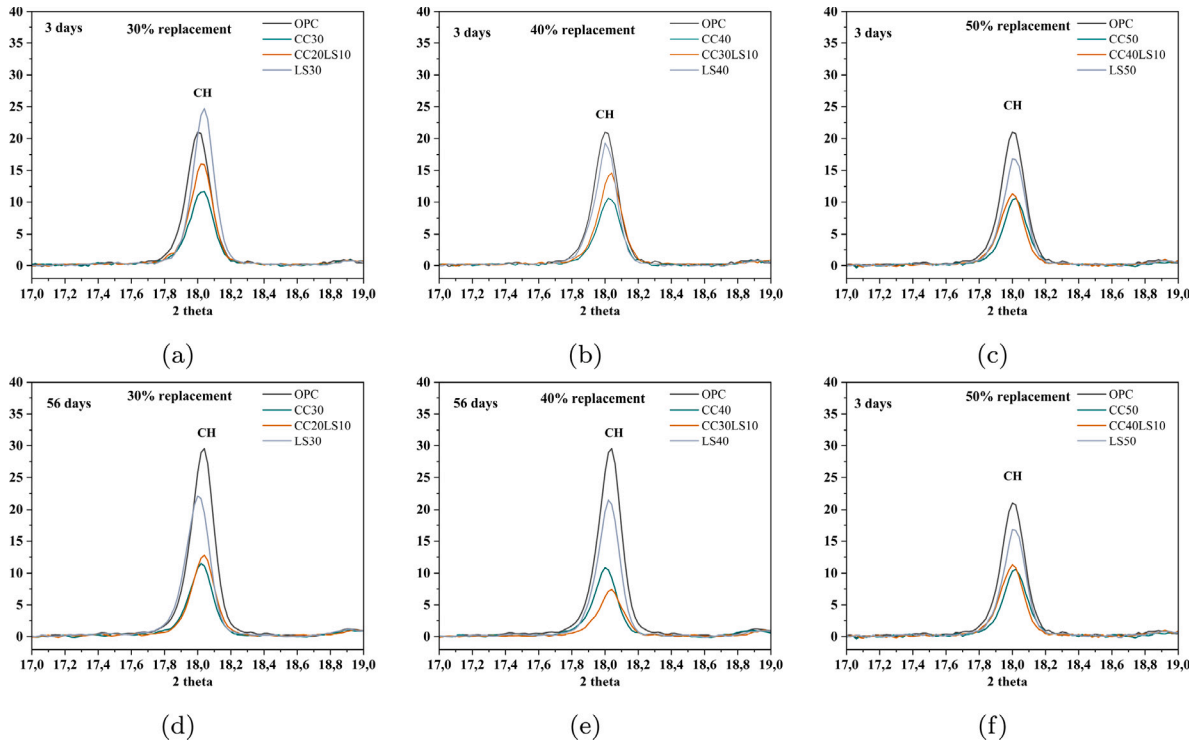

Fig. 9. Portlandite consumption of three replacements of 30%, 40% and 50% at 3 (a–c) and 56 (d–f) days.

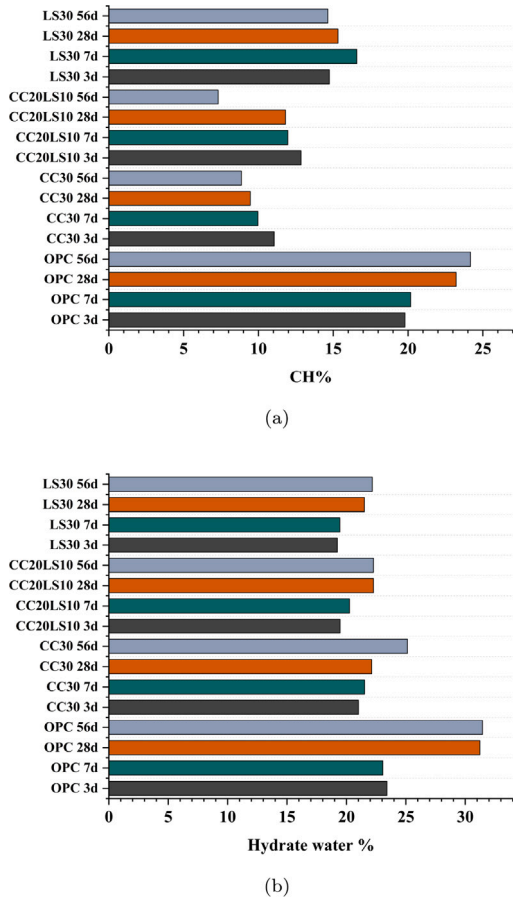

Fig. 10. Composition proportion of CH (a) and hydrate water (b), computed from mass loss curves of TGA.

At longer curing time, the reference samples shows an increase in both CH and hydrate water. The blends overall have a lower CH compared to OPC due to the substitutions. With longer hydration ages, the CH proportion decreases in all binary and ternary CC blends, indicating pozzolanic reaction to form C-(A)-S-H [63]. It has been further reported that CH is consumed to also form hemi-carbonates [60], which was detected through XRD in Fig. 8. Additionally, the proportion of hydrate water (including C-(A)-S-H, AFm, AFt, and CH) increase with time for all blended mixes, which is in agreement with the strength results. The hydrate water in OPC is highest due to the higher proportion of CH at all ages.

3.5. Structural environments of silicon and aluminum species

The ^{29}Si NMR spectra OPC and CC30 belonging to 28 and 56 days of hydration are shown in Fig. 11. It includes resonances obtained from the C-(A)-S-H phase in the range −79 to −85 ppm with roughly three main peaks corresponding to sites Q1 at around −78.5 ppm, Q2p(1 Al IV) at around −81.5 ppm, and Q2 at around −85 ppm [64]. Of these, particularly the Q2p(1 Al IV) has been reported to be associated with the incorporation of tetrahedrally coordinated Al (IV) in C-S-H, while Q2 resonating around −85 ppm contains contributions from Al-free C-S-H [46,64–66]. Comparisons of the ^{29}Si NMR spectra with 56 days old CC20LS10 are presented in Fig. D.21 in Appendix D.

Table 3 lists the calculated Al/Si ratios and mean chain lengths (MCL) of aluminosilicate tetrahedra, obtained using Eqs. (1) and (2), as reported previously in [46,47]. In CC30, the Al/Si ratio increased from 0.10 at 28 days to 0.21 at 56 days, and the MCL increased from 4.31 to 7.86, indicating progressive aluminum incorporation into the C–(A)–S–H. In contrast, OPC showed decreasing values (Al/Si 0.11 → 0.06; MCL 4.83 → 3.43).

Fig. 12 shows the ^{27}Al MAS NMR spectra for OPC and CC30 at 28 and 56 days. Corresponding comparisons for CC20LS10 at 56 days are shown in Fig. D.22 in Appendix D. The octahedral region (0–20 ppm) includes peaks for ettringite (AFt, around 15 ppm) and AFm (around 10–11 ppm), while the tetrahedral region (60–71 ppm) represents

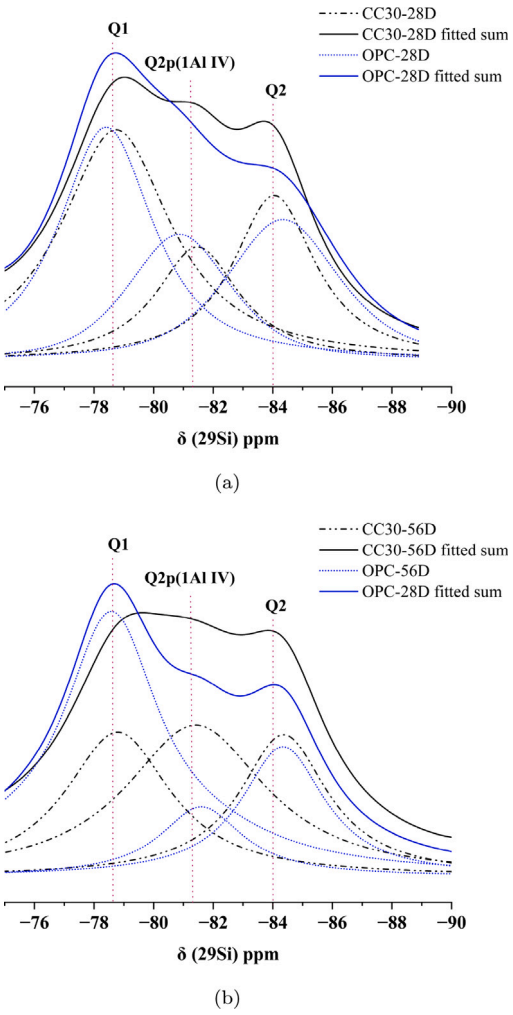

Fig. 11. ^{29}Si NMR spectra of hydrated CC30 and OPC blend aged 28 days (a) and 56 days (b). The solid lines correspond to sum of individual peaks shown by dashed lines of resonances for Q1, Q2p (1AlIV) and Q2 sites.

Table 3
Al/Si ratios and mean aluminosilicate chain lengths (MCL) of the two mixes at 28 and 56 days.

Mix	Al/Si	MCL
OPC 28D	0.1	4.8
CC30 28D	0.1	4.3
OPC 56D	0.0	3.4
CC30 56D	0.2	7.8

Al(IV) sites in C–(A)–S–H. At 28 days, the AFt resonance is stronger in CC30 than OPC, but decreases by 56 days, while the 71 ppm C–(A)–S–H signal increases. A minor resonance appears at 60–61 ppm in CC30, not seen in OPC, which could indicate limited formation of a secondary aluminosilicate phase. In case of the ternary binder CC20LS10 of 56 days, the signature intensities corresponding to AFm, AFt and C-(A)-S-H are relatively lower than for both OPC and CC30 at the same age. This can be inferred from the comparatively lower availability of alumina due to the higher OPC substitution rate.

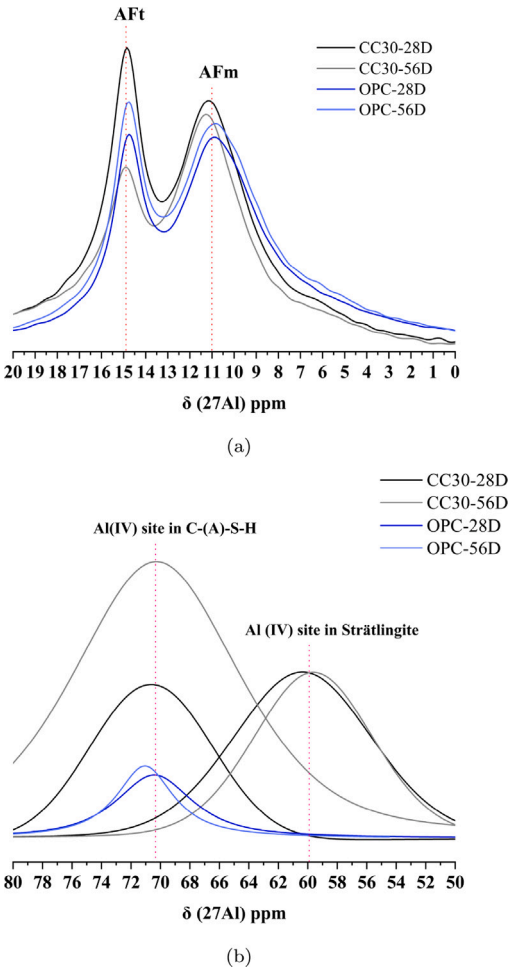

Fig. 12. ^{27}Al NMR Resonance for Al(6) sites corresponding to AFt and AFm (a), and Al(4) sites corresponding to C-(A)-S-H and Strätlingite (b).

4. Discussion

The results presented above help to address four key research questions on the hydration behavior of low-kaolinite clay blends examined in this study. The following sections discuss these questions in detail by analyzing the influence of activation on blend design, strength development, pore structure evolution, and reaction kinetics, as well as the synergy of clay with limestone and the associated alumina incorporation pathways.

4.1. What is the interplay between activation, binder design and evolution of hydration properties?

The strength and microstructural development of the studied binders demonstrate a clear interplay between the activation method, binder composition, and hydration evolution. In this study, the strength levels observed are higher than those reported in previous studies using low-kaolinite clays that were either calcined, or mechanochemically activated [9,22,67]. In another study by [68], it was concluded that in both binary and ternary systems, optimal replacement depends on the clay's alumina content. For example, it was reported in this study that replacing 30% of OPC with clay was found to need 30% alumina in the clay to match the 28-day strength of OPC. However, the results of the present study do not concur with this finding, as the clay used here contains much less alumina.

Similarly, in previous studies, pore structure evolution in cement blends containing low-kaolinite or 2:1-type clays has generally been

reported to be slower and less effective than in kaolinite-rich systems. Fernandez et al. [16] showed that pastes with calcined kaolinite clays had lower capillary porosity than OPC, whereas 2:1 clay blends exhibited higher porosity. Tironi et al. [69] likewise found that kaolinite clays developed denser microstructures than bentonite mixes due to earlier AFm formation. The RILEM TC-282 CCL report [68] similarly emphasized that pore refinement and densification depend strongly on clay reactivity and alumina content. Avet and Scrivener [10] observed that blends with more than 65% kaolinite achieved significant pore refinement within 3 days and denser microstructures by 28 days, while systems based on illitic or mixed-layer clays showed slower and more limited refinement [16,33,69]. The present results, however, indicate a pronounced and time-dependent pore refinement even though the clay used contained only around 21% kaolinite.

A likely differentiator in this case is the activation method used. In an earlier study by the present authors [36], a combined thermal (800 °C) and mechanochemical activation (500 rpm, ball-to-powder ratio of 25) was shown to significantly enhance the clay's physicochemical properties. This dual activation enabled complete dehydroxylation of all heterogenous clay mineral phases, which is typically difficult to achieve through calcination or mechanochemical activation alone. As a result, the clay exhibited a high degree of amorphousness (approximately 83%). Additionally, intensive grinding increased the BET surface area to 19 m^2/g and reduced the particle size (d50 of 16 μm). These improvements collectively raised the clay's pozzolanic reactivity from nearly inert when only calcined or only mechanochemically activated, to moderately reactive under combined activation.

In this context, the strength development of binary clay blends in the current study matches or exceeds that of blends using pure kaolinite calcined clays [16], or clays with at least 40% kaolinite [68]. The overall high structural disorder across all mineral phases achieved through the activations likely contributes to this performance. Earlier, Tole et al. and Marsh et al. [27,70] have observed long range disorder in the aluminosilicate structure of 2:1 minerals, because of mechanochemical activation. Such enhanced dehydroxylation of smectites and illites increases the dissolution rate of its aluminum in alkaline environments, facilitating greater aluminum incorporation into the C-(A)-S-H phase [32]. This is consistent with the elevated levels of Al (IV) sites associated with C-(A)-S-H observed in NMR analysis, corresponding to higher Al/Si as well as higher polymerization at 56 days.

This densification is mirrored in the evolution of the pore structure. Mercury intrusion porosimetry shows a progressive decrease in total porosity for all mixes, with the most pronounced refinement in CC30, which exhibited a 42% reduction between 3 and 56 days. While the total early-age porosity remained higher than OPC, blends CC20, CC30, CC20LS10, and CC30LS10 exhibited a higher proportion of gel or micro-pores at 3 days compared to OPC. This indicates early pore refinement and possible enhancement in C–S–H formation due to dilution and nucleation effects from the finer SCM particles, similar to observations for kaolinite-rich clays [8]. By 7 days, this refinement is strongly reflected in strength improvements, with CC30 already surpassing OPC while maintaining a higher fraction of fine pores. In contrast, higher-replacement or ternary blends such as CC40 and CC40LS10 also show increased micro-pore content but retain a greater fraction of interconnected larger pores, offsetting strength gains. At later ages (28–56 days), the correlation between gel pore development and strength becomes even stronger, particularly for CC20 and CC30. The 30% binary blend (CC30) exhibited a 42% reduction in total porosity by 56 days. Compared with kaolinite-rich LC_3 systems where rapid aluminate release promotes early carboaluminate formation and rapid capillary pore filling within 3 days [8], the pore refinement in the present low-kaolinite systems progresses more gradually but consistently, ultimately achieving substantial densification that aligns with improved strength. Hydrate phase characterizations confirm sustained aluminosilicate reactivity and ongoing gel polymerization, as also supported by the NMR evidence showing increasing Al incorporation and chain polymerization in C-(A)-S-H at 56 days.

However, since not all CH was consumed by 56 days as noticed from the XRD spectra, it cannot be concluded that the enhanced strength is solely from the pozzolanic reaction of the clay. The strength gains are likely the result of a combined effect: high reactivity of the clay minerals, fine particle size distribution (PSD), and high specific surface area. In addition to improved clinker reactivity through dilution, the fine PSD of the clay contributed to filler effects, while the large surface area accelerated early-age reaction kinetics. The higher surface area also likely provided nucleation sites that supported the formation of ettringite and AFm phases [71], which are typically delayed or unstable in heterogeneous clay systems. The filler and nucleation effects further help densify the pore structure, leading to higher strength.

Regarding optimal mixes from the studied matrix, Fig. A.14 shows strength relative to OPC, at the 4 ages corresponding to the blends studied. At 7 days, the optimum replacement is found to be 20 to 30% of binary substitution by clay. At 28 and 56 days, the optimum replacements are 20%–40% of clay substitution, as well as ternary with 20%–30% clay and 10% limestone respectively. Substitutions of 50% binary blends reached 87% of OPC strength by 28 days, while CC40LS10 reached 81% of OPC strength by 56 days. Depending on performance requirements, the activated clay can therefore be used effectively even at these high replacement levels.

Although compressive strengths of blends with replacement above 40% are considered relatively lower than CEM I binders (e.g., < 56 MPa at 28 days), such systems can still meet mechanical performance requirements under certain conditions. According to EN 206:2013+A2:2021 [72] and EN1992-1-1:2005 [73], minimum strength classes (e.g., C30/37 or C25/45) are suitable for most standard structural applications, particularly in residential and light commercial construction, provided the exposure class requirements (e.g., XC, XF, XA) are satisfied through appropriate durability assessments. These provisions open pathways for activated heterogenous blends even with higher cement substitution to be applied in mass concreting, pavements, or structures in non-aggressive environments [74].

4.2. How does the binder design influence synergy of the activated clay with limestone?

The strength results observed here contrast with findings from previous studies on calcined high-kaolinite LC3 systems [5,9,10,40,42,50], where synergistic interactions between limestone and aluminates from calcined clay typically led to improved mechanical performance compared to binary blends. According to existing literature, this difference is likely due to the lower alumina in the clay used in this study, which restricts additional carboaluminate formation after limestone addition in the ternary blends. Although XRD confirms the presence of stable, space-filling CO_3-AFm phases in the ternary blends, NMR results suggest that C–(A)–S–H and AFm phases compete for available aluminum. Fig. D.22 shows that preferential Al incorporation in C-(A)-S-H over AFms occur in ternary binders too, as observed for CC20LS10.

The strength difference between binary and ternaries is particularly major in the early ages. In this stage, the primary contributing factor may be the relatively coarser particle size distribution of the limestone used, compared to the finer limestone used in the referenced studies [10,41,56]. Coarser limestone has a lower surface area, which reduces nucleation potential [57]. Moreover, it dissolves more slowly, delaying the availability of carbonate ions needed to react with the alumina supplied by the clay [75]. By the time that carbonates are available for sufficient AFms, Al ions could already be incorporated in C-(A)-S-H.

From Fig. 7 it is observed that LS-F highly accelerate early reaction kinetics of C3S leading to fast depletion of sulfates [42]. The cumulative heat evolution follows the order of fineness, as coarser

limestone delays the hydration of aluminates [76]. However, while these PSD-related limitations predominantly affect early-age hydration and strength development, their influence tends to diminish over time. Previous studies [76,77] have shown that the impact of limestone fineness on strength plateaus at later ages as the slower dissolution of coarser particles eventually compensates for the initial delay. As observed in Fig. 7(b), after around 120 h (5 days), the heat evolution of both blends with LS-M gradually overtakes the curve for LS-F. LS-L which was used for this study, also increases continuously while gradually narrowing the gap with the finer LS. This indicates slow but eventual release of carbonates that can potentially form CO_3-AFms, contributing to strength. It needs to be evaluated whether finer limestone could alter the aluminum distribution between AFm phases and C-(A)-S-H, potentially influencing not only early strength but also long-term pore structure and durability. This aligns with the observed later strength development in CC20LS10 and CC30LS10, both of which are slow in the beginning but reach strengths comparable to OPC by 28 and 56 days, while still continuing to refine the pore structure.

Nevertheless, the remaining ternary blends, although showing continued strength gains over time, did not reach OPC-equivalent strength at any age. Simultaneously, no significant improvement of the pore structure was observed, particularly for blends with 20% limestone additions. This may suggest that the delayed reactivity of coarser limestone can only partially compensate for early-age strength limitations. For improving this synergy, future studies can look into limestone fineness and purity, use of additional sulfates, grinding aids, ratio of activated clay to limestone could be crucial parameters.

4.3. What are the pathways for aluminum in activated low-kaolinite blends?

The NMR results provide new insight into the hydration mechanism of activated low-kaolinite, 2:1-rich clays. Previous research established that such systems result in limited CO_3–AFm phases due to their low reactive alumina content [6,8,10,35], but the fate of the dissolved Al remained unresolved. The present data clarify that this limited aluminum is not inert but preferentially incorporated into the C–(A)–S–H structure, which also explains the enhanced gel polymerization observed in these systems.

The increase in Al/Si ratio from 0.10 to 0.21 and the mean chain length (MCL) from 4.31 to 7.86 between 28 and 56 days for CC30 show progressive Al substitution into the silicate chains of C–(A)–S–H, consistent with the tetrahedral coordination reported for similar systems [46,47,64]. In contrast, OPC exhibits decreasing Al/Si (0.11 → 0.06) and MCL (4.83 → 3.43), indicating depolymerization of the C–S–H with age [66]. This aligns with the limited CO_3–AFm intensities seen in XRD and TGA with the increasing C-(A)-S-H polymerization detected by NMR. The sustained Al uptake into the gel could refine pore structure, contributing to the observed late-age densification and strength gain, consistent with correlations reported for C–(A)–S–H in blended systems [12,46,48].

The ^{27}Al resonance near 60–61 ppm, observed only in CC30 and CC20LS10, could potentially correspond to strätlingite, as previously identified in cementitious systems where tetrahedral Al is linked to Si in a 1:1 layer structure [47,78,79]. Strätlingite was however not detected in XRD, most likely due to its inherently low crystallinity [80]. The appearance of this signal imply that part of the dissolved Al participates in localized Al–Si ordering beyond the C–(A)–S–H phase.

The presence of strätlingite is usually linked to the depletion of calcium hydroxide as these two phases are thermodynamically incompatible [78]. However, from the TGA (Fig. 10a), it is inferred that CH was still present in 56 days CC30 blend. It is known that strätlingite can be formed at relatively high Al and Si concentrations contributed by blended high kaolinite clays, and it can co-exist with CH, due to local heterogeneity of the hydrated matrix [78,79]. Current results for CC30 indicate that the metakaolin content alone may not govern the formation of strätlingite. Thermodynamical and NMR studies by Myers et al. [81] and Henning et al. [82] detected Strätlingite in cement blends substituted by alkali activated low alumino-silicate SCMs, such as slags and fly ash. Previous studies have linked the presence of strätlingite with higher degree of reaction (DoR) of SCMs [48]. Although the detected quantity in this study is minor, its presence supports the interpretation that progressive aluminosilicate reactivity in the activated clay promotes both Al incorporation into C–(A)–S–H and secondary strätlingite formation at later ages. Nevertheless, this signal is not interpreted as conclusive evidence of strätlingite formation. Rather, it is discussed as a possible indication of locally favorable Al–Si environments, supporting the interpretation of enhanced aluminosilicate reactivity in the activated clay system.

Overall, these results demonstrate that in activated low-kaolinite clays, the limited reactive alumina preferentially enters C–(A)–S–H, enhancing its polymerization instead of stabilizing CO_3–AFm phases. This gel-driven refinement mechanism contrasts with kaolinite-rich LC_3 systems, where abundant reactive alumina promotes early carboaluminate formation and faster matrix refinement [8,10]. Understanding this aluminum incorporation pathway clarifies the broader picture of hydration in low-alumina clays and clarifies their distinctive microstructural evolution.

4.4. What is the role of binder design on the need for sulfate adjustment?

In aluminate rich clay binders, it is known that the early sulfate depletion leads to an accelerated and enhanced aluminate reaction which causes the second peak to superimpose on the alite (C_3S or silicate peak [55]. As a result, the guidelines for mix designs with clay suggest adjusting the sulfate content for avoiding poor early age strength development [8]. The need for sulfate adjustment was evaluated for the current binder proportions through isothermal calorimetry.

In the current results (Fig. 6), except for the blends with 50% OPC replacements, the aluminate peak does not superimpose on the C_3S peak, indicating that retardation by addition of extra gypsum may not be necessary. Blends CC50 and CC40LS10 may show under sulfation driven by the high replacement ratio. The reason why the CC blends up to 40% replacements do not experience significant under-sulfation could be two-fold. Firstly, a relatively higher amount of SO_3 is already present in the cement (3.5%) than in clinkers used elsewhere (1–1.5%), such as in [42,56,67]. To some extent, this could compensate for the high adsorption of sulfates during C-(A)-S-H precipitation in the acceleration period. Secondly, the amount of alumina in the clay in this study is less than kaolinite rich clays used in LC3 studies previously. The role of clay's alumina content in dominating accelerated sulfate depletion by controlling the silicate reaction, has been established through various mechanisms as reported in [10,55,67]. For the relatively lower alumina in the clay, the existing gypsum from the cement may be adequate for preventing significant under sulfation.

The cumulative heat evolution curves for the blends demonstrate continuous increase in heat release till the end of measurement (7 days). Comparatively, the OPC curve majorly stabilizes after approximately 48 h. This indicates ongoing contributions from pozzolanic reactions in blends beyond their initial acceleration at early hours which are potentially from filler and dilution effects [57]. As a result, the adverse impact of reduced sulfate availability on early strength development in the blends was not significant. Compressive strength tests showed that both binary and ternary clay-based systems with up to 40% OPC replacement achieved at least 80% of the 7-day strength of plain OPC, despite the absence of sulfate adjustment. Among the mixes CC20, CC30, CC40, CC20LS10 and CC30LS10, the lowest 7-day strength was recorded for CC30LS10, reaching 39 ± 2 MPa. For comparison with a conventional LC3 mix, a similar 7-day strength level (40 MPa) was previously reported for a system containing clay with 60% calcined kaolinite and having 5% additional sulfate [5].

In addition to the above considerations, adding excess gypsum can react with available reactive alumina in the binder matrix for ettringite

formation, which could uptake calcium from calcium hydroxide (portlandite) [48]. This, in turn, may reduce the availability of portlandite for the pozzolanic reaction of the clays [8]. This can potentially diminish the reactivity gained through their combined activation. Based on the reaction kinetics of the current blends, it was decided not to adjust the mix designs with additional sulfates for subsequent analyses in the study. However, sulfate adjustment could be important for clays with alternative mineralogy. Especially from the perspective of enhancing the strength of higher substitutions and alternative combinations of clay and limestone, future studies on activated 2:1 clays could investigate sulfate adjustment.

5. Conclusions

This study explored the performance of blended cement systems incorporating a comprehensively activated heterogeneous clay with approximately 20% kaolinite. Using a statistically designed matrix of binary and ternary mixes, the strength development, pore structure evolution, hydrate phase assemblage, and aluminum incorporation were evaluated. The role of limestone as a complementary additive was also assessed to determine its influence on reaction kinetics and potential to support higher substitution levels.

Although blends with $\geqslant$ 40% kaolinite are known to perform well, clays with lower kaolinite content have historically shown limited reactivity and slower strength development, especially when activated by calcination alone. Mechanochemical activation has recently emerged as a promising strategy to enhance their performance, yet detailed investigations into mix design and hydration behavior remain scarce. Even with improved reactivity, low-kaolinite clays are often assumed to underperform due to their reduced alumina content and limited capacity for carboaluminate formation. This work challenges that assumption by demonstrating that, when activated through a combined thermo–mechanochemical route, low-kaolinite clays can achieve strength and microstructural refinement comparable to high-kaolinite systems. However, the hydration mechanisms differ: aluminum incorporation and limestone synergy remain less understood in these systems. It is unclear whether reactive Al in low-kaolinite blends contributes to AFm formation or is primarily integrated into the C–(A)–S–H network. Addressing this gap, the study provides new insights into how clay mineralogy and activation influence aluminum distribution and overall blend performance.

The key findings are as follows:

1. Combinedly activated low-kaolinite clay blends could demonstrate comparable or even higher strength and pore structure development as OPC, especially up to 40% replacement levels.
2. Binary blends with 20%–40% activated clay substitutions reached up to 125% of OPC strength at 56 days. This correlated with increased pore structure refinement, especially in the gel pore range, and a high C-(A)-S-H polymerization at 28 and 56 days of hydration as observed in the 30% substituted blend.
3. Limestone addition to clay mixes delayed early strength. Even though the strength continued to increase in later ages, it could not match the strength levels of binary clay mixes. ^{27}Al NMR confirmed of increasing tetrahedral aluminum incorporation over time. At later ages, Al signals remained predominantly tetrahedral, with minor octahedral Al observed, suggesting Al is largely integrated into the C-(A)-S-H network rather than forming AFm.
4. The mixes with higher proportion of clay lead to denser pore structure. Specifically, the 30% binary substitution led to 42% reduction in total porosity at 56 days. This is consistent with the modified hydrate assemblage, where progressive CH consumption and increased hydrate water (TGA), formation of Al-rich C–(A)–S–H and CO_3-AFm phases, and higher Al uptake/longer silicate chains in C-(A)-S-H (NMR) collectively refine capillary pores and densify the matrix.
5. Substitutions of 50% binary blends reached 87% of OPC strength by 28 days, while CC40LS10 reached 81% of OPC strength by 56 days. Although durability parameters remain to be investigated, based on relative strengths and pore structure refinement, binary and ternary clay mixes above 40% could still meet strength class requirements specified in standards.

CRediT authorship contribution statement

Amrita Hazarika: Writing – review & editing, Writing – original draft, Methodology, Investigation, Formal analysis, Data curation, Conceptualization. **Liming Huang:** Writing – review & editing, Supervision, Methodology. **Joao Figueira:** Investigation, Formal analysis, Data curation. **Arezou Babaahmadi:** Writing – review & editing, Supervision, Project administration, Methodology, Funding acquisition, Conceptualization.

Declaration of competing interest

The authors declare that they have no known competing financial interests or personal relationships that could have appeared to influence the work reported in this paper.

Acknowledgments

The authors acknowledge the grant offered by FORMAS, the Swedish research council, for the project: New era for cement replacement materials: Importance of service life design (NewDurCem with Grant no.: FR-2020/0008), and Family Thomas Foundation for project: Evolution of pozzolan incorporated concrete: resistance to carbonation (Carbo-crete). This work is also partially funded by Vinnova (Sweden's Innovation Agency), Grant number: 2021-01053, under the project: Towards a climate neutral and resource efficient soil stabilization additive (the work is carried out within the strategic innovation program InfraSweden2030, a joint initiative by Vinnova, Formas and the Swedish Energy Agency). The authors would like to acknowledge NMR support from the NMR Core Facility at the Swedish NMR Centre (SwedNMR, Umeå node), Umeå University and SciLifeLab. Per Lindh is acknowledged for his assistance with providing the clay samples. The authors sincerely thank Gilles Plusquellec at RISE (Research Institutes of Sweden) for assistance with a part of TGA and valuable discussions about the research. Additionally, the authors are grateful to Haitao Gu for facilitating the MIP measurements, Birhan Abdullahi Alkadir, and student assistants at Chalmers Building Materials Lab – Archanath Dickwella, Matilda Andersson, Agnes Jonsson and Amith Adhikari for helping with material preparations and experiments.

Appendix A. Compressive strength development

This appendix provides supporting data for the compressive strength results discussed in Section 3.1.

Fig. A.13 shows the evolution of compressive strength for all mixes at four curing ages (3, 7, 28, and 56 days). The results confirm that the binary clay blends, particularly CC20 and CC30, exhibit faster and greater strength development than OPC, while limestone-only blends lag behind.

Fig. A.14 compares the relative strength of the different replacement levels across all ages, highlighting the optimum substitution ranges (20%–40% clay and 10% limestone) for achieving strength levels equivalent to or higher than OPC.

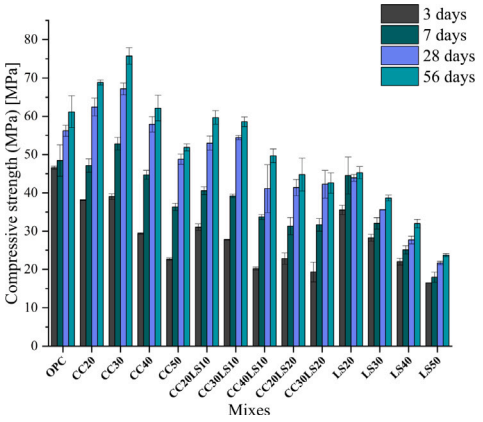

Fig. A.13. Compressive strength development of the tested mixes on four ages.

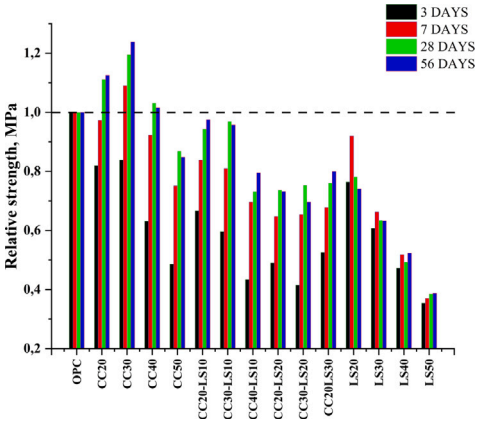

Fig. A.14. Relative strengths at various replacements and hydration ages.

Appendix B. Pore structure evolution

This appendix compliments the pore structure results presented in Section 3.2. Fig. B.15 shows the evolution of pore size distribution corresponding to mixes: CC40, CC50, CC30LS10, CC40LS10, CC20LS20, CC30LS20, CC20LS30, LS40 and LS50. Fig. B.16(a–b) shows the total porosity and total pore volumes of all mixes at different curing ages. The data demonstrate a clear decrease in both parameters over time, especially for CC30, which achieves the greatest refinement by 56 days. Fig. B.17 illustrates the statistical correlation between total porosity, total pore volume, and compressive strength. While total porosity alone does not strongly correlate with strength, the results emphasize the importance of the pore-size distribution in determining mechanical performance.

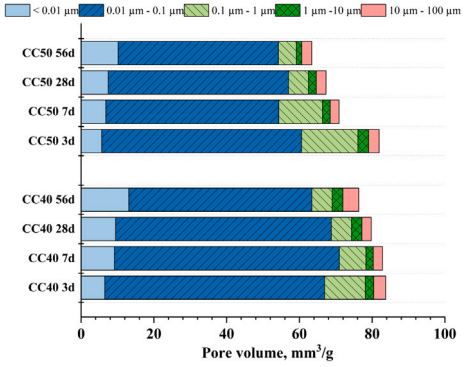

(a)

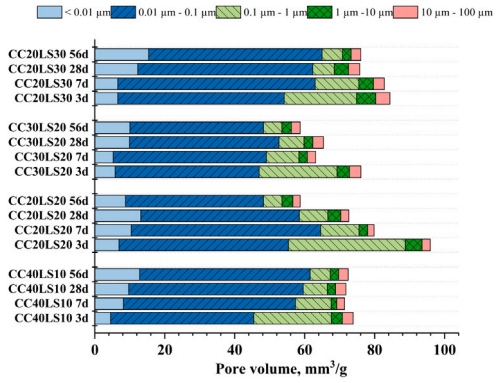

(b)

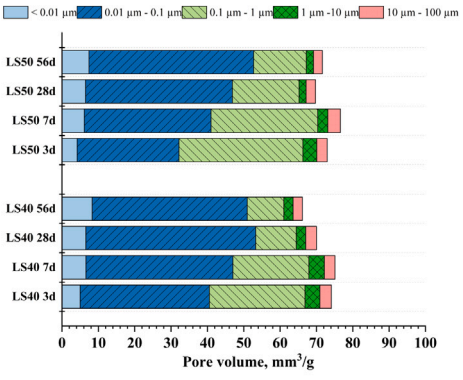

(c)

Fig. B.15. Distribution of pore volumes of reference (OPC), binary mixes with activated clay (a), ternary mixes (b), and limestone fillers (c).

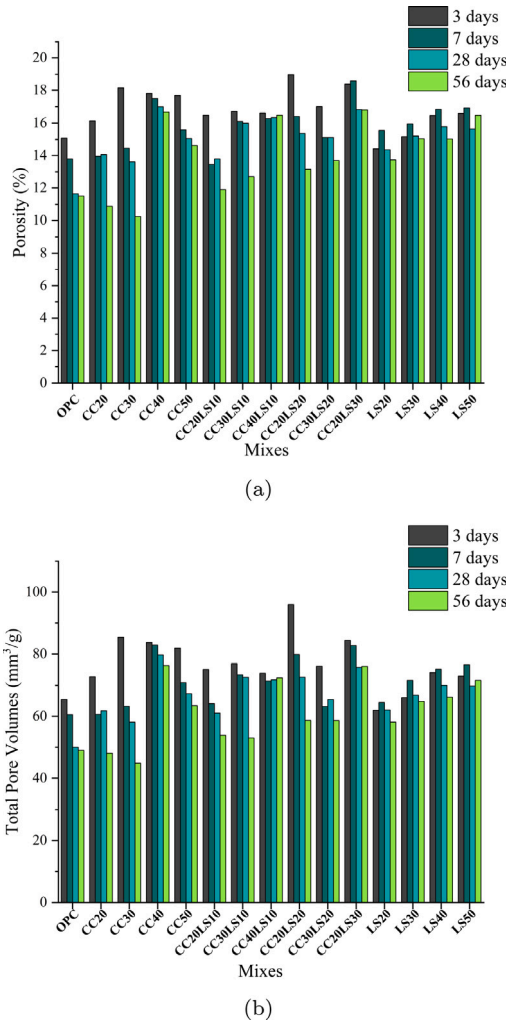

Fig. B.16. Total porosity (a) and total pore volumes (b) in four ages of the mixes.

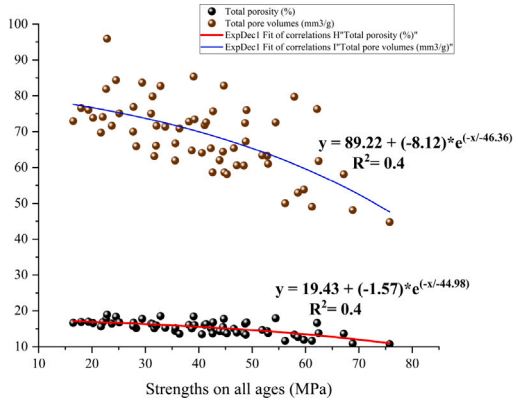

Fig. B.17. Correlation between strengths of mixes on all ages and total porosity (black scatter points), as well as total pore volumes (brown scatter points).

Appendix C. Hydrate structure characteristics

This appendix presents complementary data for the hydrate phase assemblage discussed in Section 3.4.

C.1. CO_3-AFms

Fig. C.18(a–d) shows XRD peaks corresponding to hemicarbonate (Hc) and monocarboaluminate (Mc) identified at 3, 7, 28, and 56 days. The results confirm early Hc formation followed by its gradual conversion to Mc at later ages, consistent with the stabilization of CO_3-AFm phases. It is acknowledged that reliable estimates of these CO_3-AFms could be hampered by their known ill-crystallinity as previously noted in [62].

C.2. DTG mass loss

Fig. C.19 shows the proportion of mass loss of the mixes at the four varying curing ages. Fig. C.20(a–d) presents the differential thermogravimetric (DTG) curves of the hydrated mixes over four curing ages. The characteristic mass-loss regions for CH (400–500 °C) and total hydrate water (40–520 °C) confirm ongoing hydration, while the reduction in CH-related peaks and increase in hydrate water with age correspond to progressive pozzolanic reaction and gel formation.

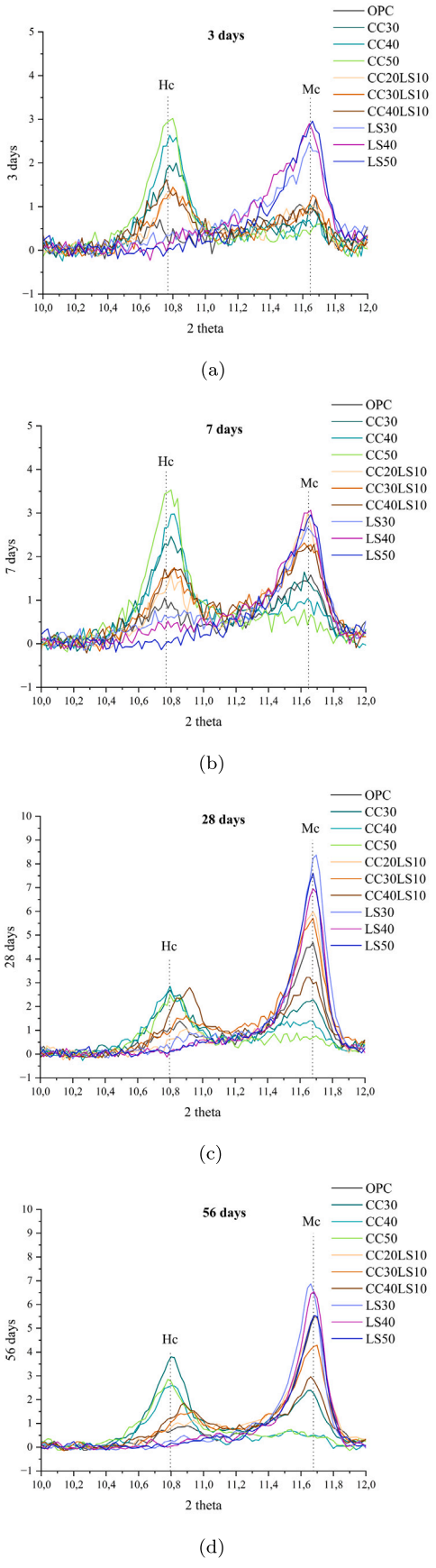

Fig. C.18. (a–d): Peaks from X-ray diffraction that correspond to Hemicarboaluminates (Hc) and Mono-carboaluminates (Mc), for the mixes on the four ages.

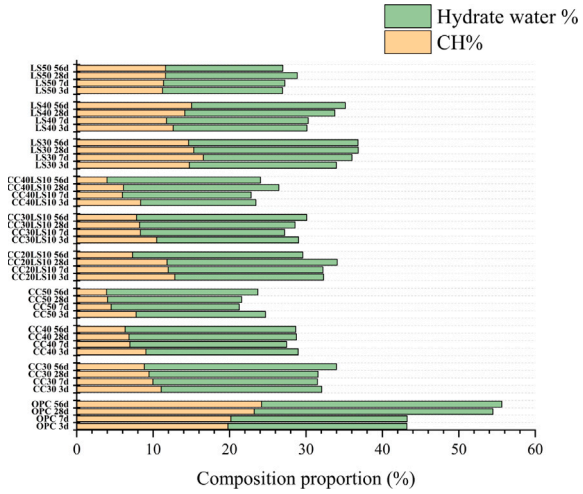

Fig. C.19. Proportion of CH and Hydrate water in all mixes studied on ages 3, 7, 28 and 56 days.

Appendix D. Aluminum incorporation in binary and ternary blends

The section presents the spectra of ^{29}Si MAS NMR of 56 days old OPC, CC30 and CC20LS10 in Fig. D.21. It is observed that the whole C-S-H spectra for CC20LS10 is considerably lower than for the other two mixes. This can be explained in conjunction with the lower aluminosilicates available in the system to promote the formation of C-S-H. Fig. D.22(a) demonstrate the ^{27}Al MAS NMR spectra correlating to AFt and AFms, and Fig. D.22(b) demonstrates the spectra corresponding to the Al (IV) sites relating to C-(A)-S-H and Strätlingite. It can be seen that CC20LS10 has much lower proportions of Al (IV) relating to C-(A)-S-H than CC30 as could be inferred from the ^{29}Si spectra as well. However, it does record slightly higher signal corresponding to Al(IV) sites that could be strätlingite.

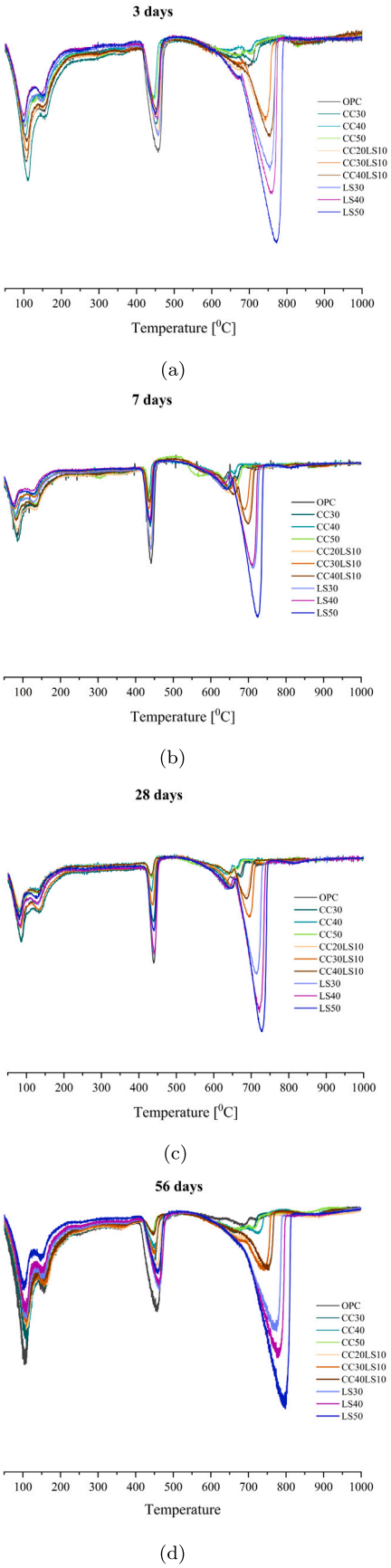

Fig. C.20. (a–d): DTG curves of the hydrated mixes on four ages.

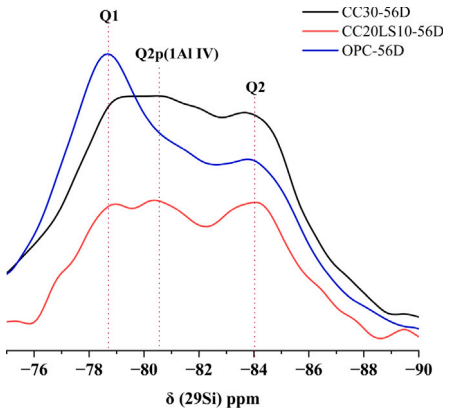

Fig. D.21. ^{29}Si NMR spectra corresponding to C-S-H or C-(A)-S-H.

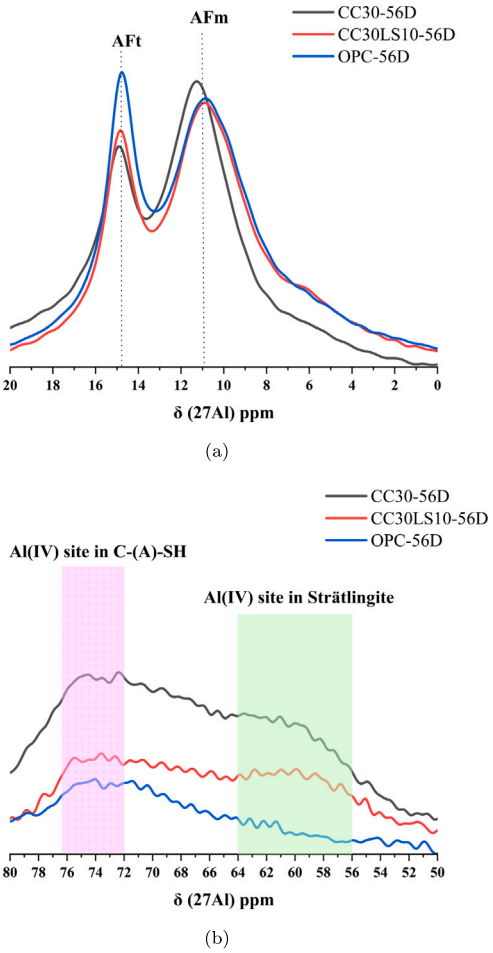

Fig. D.22. ^{27}Al NMR spectra showing Alumina sites for AFt and AFm phases (a), ^{27}Al NMR spectra for aluminum sites for C-(A)-S-H and Strätlingite phases (b) for CC30, CC20LS10 and OPC at 56 days.

Appendix E. Supplementary data

Supplementary material related to this article can be found online at https://doi.org/10.1016/j.cemconres.2025.108086.

Data availability

Data will be made available on request.

References

[1] K.L. Scrivener, V.M. John, E.M. Gartner, Eco-efficient cements: Potential economically viable solutions for a low-CO2 cement-based materials industry, Cem. Concr. Res. 114 (2018) 2–26, http://dx.doi.org/10.1016/J.CEMCONRES.2018.03.015.

[2] GCCA, Concrete future-roadmap to net zero. The GCCA 2050 cement and concrete industry roadmap for net zero concrete., 2021, p. 48, URL https://gccassociation.org/concretefuture/wp-content/uploads/2021/10/GCCA-Concrete-Future-Roadmap.pdf.

[3] K.L. Scrivener, Eco-efficient cements: No magic bullet needed, Glob. Cem. Mag. (2019) 10–14, URL https://lc3.ch/wp-content/uploads/2020/11/Ecoefficient-Cement.pdf.

[4] K. Scrivener, A. Dekeukelaere, F. Avet, L. Grimmeissen, Financial attractiveness of LC3, 2019, p. 44, URL https://lc3.ch/wp-content/uploads/2020/10/2019-LC3FinancialAttractiveness-WEB.pdf.

[5] K. Scrivener, F. Martirena, S. Bishnoi, S. Maity, Calcined clay limestone cements (LC3), Cem. Concr. Res. 114 (2018) 49–56, http://dx.doi.org/10.1016/J.CEMCONRES.2017.08.017.

[6] M. Antoni, J. Rossen, F. Martirena, K. Scrivener, Cement substitution by a combination of metakaolin and limestone, 2012, http://dx.doi.org/10.1016/j.cemconres.2012.09.006.

[7] J.N. Gonthier, W. Wilson, F. Georget, K. Scrivener, Advanced characterization of chloride binding in OPC and LC3 pastes, in: 4th International RILEM Conference on Microstructure Related Durability of Cementitious Composites (Microdurability2020), TU Delft, 2020, URL https://repository.tudelft.nl/file/File_ae4ed2f6-39ba-4fe2-a0c2-cbc0cfb2a92c?preview=1.

[8] F. Zunino, Y. Dhandapani, M.B. Haha, J. Skibsted, S. Joseph, S. Krishnan, A. Parashar, M.C. Juenger, T. Hanein, S.A. Bernal, K.L. Scrivener, F. Avet, Hydration and mixture design of calcined clay blended cements: review by the RILEM TC 282-CCL, Mater. Struct./Materiaux Constr. 55 (2022) http://dx.doi.org/10.1617/s11527-022-02060-1.

[9] F. Avet, K. Scrivener, Investigation of the calcined kaolinite content on the hydration of limestone calcined clay cement (LC3), Cem. Concr. Res. 107 (2018) 124–135, http://dx.doi.org/10.1016/J.CEMCONRES.2018.02.016.

[10] F. Avet, K. Scrivener, Investigation of the calcined kaolinite content on the hydration of limestone calcined clay cement (LC3), Cem. Concr. Res. 107 (2018) 124–135, http://dx.doi.org/10.1016/J.CEMCONRES.2018.02.016.

[11] F. Avet, K. Scrivener, Influence of pH on the chloride binding capacity of Limestone Calcined Clay Cements (LC3), Cem. Concr. Res. 131 (2020) 106031, http://dx.doi.org/10.1016/J.CEMCONRES.2020.106031.

[12] F. Zunino, K. Scrivener, Microstructural developments of limestone calcined clay cement (LC3) pastes after long-term (3 years) hydration, Cem. Concr. Res. 153 (2022) 106693, http://dx.doi.org/10.1016/J.CEMCONRES.2021.106693.

[13] T. Hanein, K.C. Thienel, F. Zunino, A.T. Marsh, M. Maier, B. Wang, M. Canut, M.C. Juenger, M.B. Haha, F. Avet, A. Parashar, L.A. Al-Jaberi, R.S. Almenares-Reyes, A. Alujas-Diaz, K.L. Scrivener, S.A. Bernal, J.L. Provis, T. Sui, S. Bishnoi, F. Martirena-Hernández, Clay calcination technology: state-of-the-art review by the RILEM tc 282-CCL, Mater. Struct./Materiaux et Constr. 55 (2022) http://dx.doi.org/10.1617/s11527-021-01807-6.

[14] A.A. Diaz, R.S.A. Reyes, T. Hanein, E.F. Irassar, M. Juenger, F. Kanavaris, M. Maier, A.T. Marsh, T. Sui, K.C. Thienel, L. Valentini, B. Wang, F. Zunino, R. Snellings, Properties and occurrence of clay resources for use as supplementary cementitious materials: a paper of RILEM TC 282-CCL, Mater. Struct./Materiaux et Constr. 55 (2022) http://dx.doi.org/10.1617/s11527-022-01972-2.

[15] R. Snellings, R. Almenares, R. Theodore, E.F. Irassar, F. Kanavaris, M. Maier, A.T. Marsh, L. Valentini, F. Zunino, A. Alujas, M. Canut, A. Castel, V. Dao, J.I. Escalante-garcia, H. Ez-zaki, F. Kanavaris, T. Kim, D. Law, A. Machner, M. Maier, F. Moro, J.M. Marangu, A. Nunes, Paper of RILEM TC 282-CCL : mineralogical characterization methods for clay resources intended for use as supplementary cementitious material, vol. 1, Springer Netherlands, 2022, http://dx.doi.org/10.1617/s11527-022-01973-1,

[16] R. Fernandez, F. Martirena, K.L. Scrivener, The origin of the pozzolanic activity of calcined clay minerals: A comparison between kaolinite, illite and montmorillonite, Cem. Concr. Res. 41 (2011) 113–122, http://dx.doi.org/10.1016/J.CEMCONRES.2010.09.013.

[17] N. Beuntner, R. Sposito, K.C. Thienel, Potential of calcined mixed-layer clays as pozzolans in concrete, ACI Mater. J. 116 (2019) 19–29, http://dx.doi.org/10.14359/51716677.

[18] A. Ahlberg, I. Olsson, P. Šimkevičius, Triassic-jurassic weathering and clay mineral dispersal in basement areas and sedimentary basins of southern Sweden, Sediment. Geol. 161 (2003) 15–29, http://dx.doi.org/10.1016/S0037-0738(02)00381-0.

[19] A. Ahlberg, U. Sivhed, M. Erlström, The jurassic of skåne, southern Sweden, Geol. Surv. Den. Greenl. Bull. 541 (2003) 527–541, http://dx.doi.org/10.34194/geusb.v1.4682.

[20] G. Plusquellec, A. Babaahmadi, U. Mueller, Activated clays as supplementary cementitious material, RISE Rep. (2020) URL https://urn.kb.se/resolve?urn=urn%3Anbn%3Ase%3Ari%3Adiva-52509.

[21] I. Tole, Enhancing the pozzolanic activity of three natural clays from Sweden by mechanochemical activation process, SSRN Electron. J. (2022) 0–2, http://dx.doi.org/10.2139/ssrn.4100172.

[22] Y. Dhandapani, K.K. Subramanian, F. Kanavaris, L. Black, S.A. Bernal, The meta-kaolinite content of the calcined clay source impacts the mechanical and durability performance of blended portland concrete, Cem. Concr. Res. 196 (2025) http://dx.doi.org/10.1016/j.cemconres.2025.107922.

[23] M. Flegar, M. Serdar, D. Londono-Zuluaga, K. Scrivener, Regional waste streams as potential raw materials for immediate implementation in cement production, Materials 13 (23) (2020) 1–15, http://dx.doi.org/10.3390/ma13235456.

[24] E.A. Costantini, D. Damiani, Clay minerals and the development of quaternary soils in central Italy, Rev. Mex. Cienc. Geol. 21 (2004) 144–159, URL https://rmcg.unam.mx/index.php/rmcg.

[25] M. Setti, A. López-Galindo, M. Padoan, E. Garzanti, Clay mineralogy in southern Africa river muds, Clay Miner. 49 (5) (2014) 717–733, http://dx.doi.org/10.1180/claymin.2014.049.5.08.

[26] A. Alujas, R. Fernández, R. Quintana, K.L. Scrivener, F. Martirena, Pozzolanic reactivity of low grade kaolinitic clays: Influence of calcination temperature and impact of calcination products on OPC hydration, Appl. Clay Sci. 108 (2015) 94–101, http://dx.doi.org/10.1016/J.CLAY.2015.01.028.

[27] A.T. Marsh, S. Krishnan, S.A. Bernal, Structural features of thermally or mechanochemically treated montmorillonite clays as precursors for alkali-activated cements production, Cem. Concr. Res. 181 (2024) http://dx.doi.org/10.1016/j.cemconres.2024.107546.

[28] A. Souri, H. Kazemi-kamyab, R. Snellings, R. Naghizadeh, F. Golestani-fard, K. Scrivener, Pozzolanic activity of mechanochemically and thermally activated kaolins in cement, Cem. Concr. Res. 77 (2015) 47–59, http://dx.doi.org/10.1016/j.cemconres.2015.04.017.

[29] V.A. Baki, X. Ke, A. Heath, J. Calabria-Holley, C. Terzi, M. Sirin, The impact of mechanochemical activation on the physicochemical properties and pozzolanic reactivity of kaolinite, muscovite and montmorillonite, Cem. Concr. Res. 162 (September) (2022) 106962, http://dx.doi.org/10.1016/j.cemconres.2022.106962.

[30] B. Luzu, M. Duc, A. Djerbi, L. Gautron, High Performance Illitic Clay-Based Geopolymer: Influence of the Mechanochemical Activation Duration on the Strength Development, in: RILEM Bookseries, vol. 25, Springer Singapore, 2020, pp. 363–373, http://dx.doi.org/10.1007/978-981-15-2806-4{_}43.

[31] C. He, E. Makovicky, B. Osbæ ck, Thermal treatment and pozzolanic activity of Na- and Ca-montmorillonite, Appl. Clay Sci. 10 (5) (1996) 351–368, http://dx.doi.org/10.1016/0169-1317(95)00037-2.

[32] N. Garg, J. Skibsted, Thermal activation of a pure montmorillonite clay and its reactivity in cementitious systems, J. Phys. Chem. C 118 (2014) 11464–11477, http://dx.doi.org/10.1021/jp502529d.

[33] K. Ram, M. Flegar, M. Serdar, K. Scrivener, Influence of low- to medium-kaolinite clay on the durability of limestone calcined clay cement (LC3) concrete, Materials 16 (2023) http://dx.doi.org/10.3390/ma16010374.

[34] N. Beuntner, Zur Eignung und Wirkungsweise calcinierter Tone als reaktive Bindemittelkomponente im Zement (Ph.D. thesis), in: Institut für Werkstoffe des Bauwesens, Fakultät für Bauingenieurwesen und Umweltwissenschaften, 6, TU Munich, 2017, URL https://nbn-resolving.org/urn:nbn:de:bvb:706-5546.

[35] N. Garg, J. Skibsted, Pozzolanic reactivity of a calcined interstratified illite / smectite, Cem. Concr. Res. (2015) http://dx.doi.org/10.1016/j.cemconres.2015.08.006.

[36] A. Hazarika, L. Huang, A. Babaahmadi, Characterisation, activation, and reactivity of heterogenous natural clays, Mater. Struct./Mat Iaux Constr. (2024) http://dx.doi.org/10.1617/s11527-024-02335-9.

[37] H. Scheffe, Experiments with mixtures, J. R. Stat. Soc. Ser. B Stat. Methodol. 20 (1957) 344–360, http://dx.doi.org/10.1111/j.2517-6161.1958.tb00299.x.

[38] N.R. Draper, W. Lawrence, Mixture Designs for Three Factors, Technical Report 3, 2018, http://dx.doi.org/10.1111/j.2517-6161.1965.tb00604.x.

[39] J.W. Gorman, J.E. Hinman, Simplex lattice designs for multicomponent systems, Technometrics 4 (1962) 463–487, http://dx.doi.org/10.1080/00401706.1962.10490034.

[40] J. Sun, F. Zunino, K. Scrivener, Hydration and phase assemblage of limestone calcined clay cements (LC3) with clinker content below 50 %, Cem. Concr. Res. 177 (2024) 107417, http://dx.doi.org/10.1016/j.cemconres.2023.107417.

[41] T. Matschei, B. Lothenbach, F.P. Glasser, The role of calcium carbonate in cement hydration, Cem. Concr. Res. 37 (2007) 551–558, http://dx.doi.org/10.1016/j.cemconres.2006.10.013.

[42] F. Zunino, Limestone calcined clay cements (LC3): raw material processing, sulfate balance and hydration kinetics, 2020, p. 212, URL http://infoscience.epfl.ch/record/277799.

[43] Svensk Standard ss-en 196-1:2016, Technical Report, Swedish Standards Institute (SIS), Stockholm, Sweden, 2016, URL https://www.sis.se/en/produkter/construction-materials-and-building/construction-materials/cement-gypsum-lime-mortar/ssen19612005/.
[44] B.M. Fung, A.K. Khitrin, K. Ermolaev, An Improved Broadband Decoupling Sequence for Liquid Crystals and Solids, Technical Report, 2000, URL http://www.idealibrary.com.
[45] T. O'Haver, Keyboard operated peak fitting function for time-series signals, ipf(arg1,arg2,arg3,arg4), MATLAB Central File Exchange., in: Matlab Central File Exchange, 2025, URL.
[46] Z. Dai, T.T. Tran, J. Skibsted, Aluminum incorporation in the C-s-h phase of white portland cement-metakaolin blends studied by 27 al and 29 si MAS nmr spectroscopy, J. Am. Ceram. Soc. 97 (2014) 2662–2671, http://dx.doi.org/10.1111/jace.13006.
[47] S. Nie, J. Skibsted, Aluminum distribution in C-(a)-S-H and calcium aluminate hydrate phases of portland cement – metakaolin – limestone blends studied by 27Al and 29Si NMR spectroscopy, Cem. Concr. Res. 186 (2024) http://dx.doi.org/10.1016/j.cemconres.2024.107664.
[48] F. Zunino, K. Scrivener, The reaction between metakaolin and limestone and its effect in porosity refinement and mechanical properties, Cem. Concr. Res. 140 (2021) 106307, http://dx.doi.org/10.1016/j.cemconres.2020.106307.
[49] D.C. Montgomery, Design and Analysis of Experiments, John Wiley & Sons, Inc., 2017, URL https://www.wiley.com/en-us/Design+and+Analysis+of+Experiments%2C+10th+Edition-p-9781119492443.
[50] M. Antoni, Investigation of cement substitution by blends of calcined clays and limestone (Ph.D. thesis), PhD, 2013, p. 254, URL https://infoscience.epfl.ch/entities/publication/9dc76224-f02e-41ff-80f6-df8f5f33e989.
[51] P. Zuschlag, The impact of curing temperatures on Portland composite cements – hydrate assemblage, porosity, and compressive strength (Ph.D. thesis), Norwegian University of Science and Technology, Trondheim, 2022, URL https://ntnuopen.ntnu.no/ntnu-xmlui/handle/11250/3042301.
[52] P.J.M.P. Mehta, Concrete microstructure, properties, and materials, 2006, http://dx.doi.org/10.1036/0071462899.
[53] R. Kumar, B. Bhattacharjee, Porosity, pore size distribution and in situ strength of concrete, Cem. Concr. Res. 33 (2003) 155–164, http://dx.doi.org/10.1016/S0008-8846(02)00942-0.
[54] E. Berodier, K. Scrivener, Evolution of pore structure in blended systems, Cem. Concr. Res. 73 (2015) 25–35, http://dx.doi.org/10.1016/j.cemconres.2015.02.025.
[55] F. Zunino, K. Scrivener, Cement and Concrete Research Insights on the role of alumina content and the filler effect on the sulfate requirement of PC and blended cements, Cem. Concr. Res. 160 (April) (2022) 106929, http://dx.doi.org/10.1016/j.cemconres.2022.106929.
[56] E. Berodier, K. Scrivener, Understanding the filler effect on the nucleation and growth of C-s-h, J. Am. Ceram. Soc. 97 (2014) 3764–3773, http://dx.doi.org/10.1111/jace.13177.
[57] B. Lothenbach, K. Scrivener, R.D. Hooton, Supplementary cementitious materials, Cem. Concr. Res. 41 (12) (2011) 1244–1256, http://dx.doi.org/10.1016/J.CEMCONRES.2010.12.001.
[58] V.S. Ramachandran, Thermal analyses of cement components hydrated in the presence of calcium carbonate, Thermochim. Acta 127 (1988) 385–394, URL https://publications-cnrc.canada.ca/eng/view/ft/?id=3ac62400-50b9-426c-873e-ea15b2acafd1.
[59] J. Péra, S. Husson, B. Guilhot, Influence of Finely Ground Limestone on Cement Hydration, Technical Report 2, 1999, http://dx.doi.org/10.1016/S0958-9465(98)00020-1.
[60] K.D. Weerdt, M.B. Haha, G.L. Saout, K.O. Kjellsen, H. Justnes, B. Lothenbach, Hydration mechanisms of ternary portland cements containing limestone powder and fly ash, Cem. Concr. Res. 41 (2011) 279–291, http://dx.doi.org/10.1016/j.cemconres.2010.11.014.
[61] M. Zajac, A. Rossberg, G.L. Saout, B. Lothenbach, Influence of limestone and anhydrite on the hydration of portland cements, Cem. Concr. Compos. 46 (2014) 99–108, http://dx.doi.org/10.1016/j.cemconcomp.2013.11.007.
[62] B. Lothenbach, G.L. Saout, E. Gallucci, K. Scrivener, Influence of limestone on the hydration of portland cements, Cem. Concr. Res. 38 (2008) 848–860, http://dx.doi.org/10.1016/j.cemconres.2008.01.002.
[63] F. Avet, X. Li, K. Scrivener, Determination of the amount of reacted metakaolin in calcined clay blends, Cem. Concr. Res. 106 (2018) 40–48, http://dx.doi.org/10.1016/J.CEMCONRES.2018.01.009.
[64] S.Y. Yang, Y. Yan, B. Lothenbach, J. Skibsted, Incorporation of sodium and aluminum in cementitious calcium-alumino-silicate-hydrate C-(a)-s-h phases studied by 23na, 27al, and 29si MAS nmr spectroscopy, J. Phys. Chem. C 125 (2021) 27975–27995, http://dx.doi.org/10.1021/acs.jpcc.1c08419.
[65] J. Skibsted, E. Henderson, H.J. Jakobsen, Characterization of Calcium Alumínate Phases in Cements by 27A1 MAS NMR Spectroscopy, Technical Report, 1993, URL https://pubs.acs.org/sharingguidelines.
[66] M.D. Andersen, H.J. Jakobsen, J. Skibsted, Incorporation of aluminum in the calcium silicate hydrate (c-s-h) of hydrated portland cements: A high-field 27Al and 29si MAS NMR investigation, Inorg. Chem. 42 (2003) 2280–2287, http://dx.doi.org/10.1021/ic020607b.
[67] M.R.C. da Silva, J. da Silva Andrade Neto, B. Walkley, A.P. Kirchheim, Effects of kaolinite and montmorillonite calcined clays on the sulfate balance, early hydration, and artificial pore solution of limestone calcined clay cements (LC3), Mater. Struct./Materiaux Constr. 57 (2024) http://dx.doi.org/10.1617/s11527-024-02462-3.
[68] S. Joseph, Y. Dhandapani, D.A. Geddes, Z. Zhao, S. Bishnoi, M. Vieira, F. Martirena, A. Castel, F. Kanavaris, T. Bansal, K.A. Riding, Mechanical properties of concrete made with calcined clay: a review by RILEM TC-282 CCL, Mater. Struct./Materiaux Constr. 56 (2023) http://dx.doi.org/10.1617/s11527-023-02118-8.
[69] A. Tironi, M.A. Trezza, A.N. Scian, E.F. Irassar, Assessment of pozzolanic activity of different calcined clays, Cem. Concr. Compos. 37 (2013) 319–327, http://dx.doi.org/10.1016/j.cemconcomp.2013.01.002.
[70] I. Tole, F. Delogu, E. Qoku, K. Habermehl-Cwirzen, A. Cwirzen, Enhancement of the pozzolanic activity of natural clays by mechanochemical activation, Constr. Build. Mater. 352 (August) (2022) http://dx.doi.org/10.1016/j.conbuildmat.2022.128739.
[71] M. Maier, S. Scherb, A. Neißer-Deiters, N. Beuntner, K.C. Thienel, Hydration of cubic tricalcium aluminate in the presence of calcined clays, J. Am. Ceram. Soc. 104 (7) (2021) 3619–3631, http://dx.doi.org/10.1111/jace.17745.
[72] Svensk Standard SS-EN 206:2013+A2:2021 Concrete-Specification, Performance, Production and Conformity, Technical Report, 2021, URL https://www.sis.se/en/produkter/construction-materials-and-building/construction-materials/concrete-and-concrete-products/ss-1370032021/.
[73] Svensk standard SS-EN1992-1-1:2005 Eurocode 2: Design of concrete structures-Part 1-1: General rules and rules for buildings, Technical Report, 2005, URL https://www.sis.se/en/produkter/construction-materials-and-building/construction-industry/technical-aspects/ssen1992112005/.
[74] R. Kurda, J. de Brito, J.D. Silvestre, Concretop - a multi-criteria decision method for concrete optimization, Environ. Impact Assess. Rev. 74 (2019) 73–85, http://dx.doi.org/10.1016/j.eiar.2018.10.006.
[75] F.E. Bear, L. Allen, Relation between fineness of limestone particles and their rates of solution, Ind. Eng. Chem. 24 (1932) 998–1001, http://dx.doi.org/10.1021/ie50273a008.
[76] Y. Briki, M. Zajac, M.B. Haha, K. Scrivener, Impact of limestone fineness on cement hydration at early age, Cem. Concr. Res. 147 (2021) 106515, http://dx.doi.org/10.1016/j.cemconres.2021.106515.
[77] L.M.V. Andrés, M.G. Antoni, A.A. Diaz, J.F.M. Hernández, K.L. Scrivener, Effect of fineness in clinker-calcined clays-limestone cements, Adv. Cem. Res. 27 (2015) 546–556, http://dx.doi.org/10.1680/adcr.14.00095.
[78] W. Kunther, Z. Dai, J. Skibsted, Thermodynamic modeling of hydrated white portland cement-metakaolin-limestone blends utilizing hydration kinetics from 29si mas NMR spectroscopy, Cem. Concr. Res. 86 (2016) 29–41, http://dx.doi.org/10.1016/j.cemconres.2016.04.012.
[79] B. Lothenbach, M. Zajac, Application of thermodynamic modelling to hydrated cements, Cem. Concr. Res. 123 (2019) 105779, http://dx.doi.org/10.1016/j.cemconres.2019.105779, URL https://www.sciencedirect.com/science/article/pii/S0008884619301383.
[80] B. Lothenbach, T. Matschei, G. Möschner, F.P. Glasser, Thermodynamic modelling of the effect of temperature on the hydration and porosity of Portland cement, Cem. Concr. Res. 38 (1) (2008) 1–18, http://dx.doi.org/10.1016/j.cemconres.2007.08.017.
[81] R.J. Myers, B. Lothenbach, S.A. Bernal, J.L. Provis, Thermodynamic modelling of alkali-activated slag cements, Appl. Geochem. 61 (2015) 233–247, http://dx.doi.org/10.1016/j.apgeochem.2015.06.006.
[82] R. Henning, P. Sturm, D.A. Geddes, S. Keßler, B. Walkley, G.J. Gluth, The influence of curing temperature on the strength and phase assemblage of hybrid cements based on GGBFS/FA blends, Front. Mater. 9 (2022) http://dx.doi.org/10.3389/fmats.2022.982568.